TKK Dissertations 252
Espoo 2010

CVD SYNTHESIS OF CARBON NANOMATERIALS

Doctoral Dissertation

Prasantha Reddy Mudimela

Aalto University
School of Science and Technology
Faculty of Information and Natural Sciences
Department of Applied Physics

TKK Dissertations 252
Espoo 2010

CVD SYNTHESIS OF CARBON NANOMATERIALS

Doctoral Dissertation

Prasantha Reddy Mudimela

Doctoral dissertation for the degree of Doctor of Science in Technology to be presented with due permission of the Faculty of Information and Natural Sciences for public examination and debate in Auditorium Y124 at the Aalto University School of Science and Technology (Espoo, Finland) on the 18th of November 2010 at 13 o'clock.

Aalto University
School of Science and Technology
Faculty of Information and Natural Sciences
Department of Applied Physics

Aalto-yliopisto
Teknillinen korkeakoulu
Informaatio- ja luonnontieteiden tiedekunta
Teknillisen fysiikan laitos

Distribution:
Aalto University
School of Science and Technology
Faculty of Information and Natural Sciences
Department of Applied Physics
P.O. Box 11100 (Otakaari 1 M)
FI - 00076 Aalto
FINLAND
URL: http://tfy.tkk.fi/
Tel. +358-9-470 23153
Fax +358-9-470 23155
E-mail: prasantha.reddy@tkk.fi

ISBN 978-952-60-3454-6
ISBN 978-952-60-3455-3 (PDF)
ISSN 1795-2239
ISSN 1795-4584 (PDF)
URL: http://lib.tkk.fi/Diss/2010/isbn9789526034553/

TKK-DISS-2838

Multiprint Oy
Espoo 2010

Aalto University

ABSTRACT OF DOCTORAL DISSERTATION	AALTO UNIVERSITY SCHOOL OF SCIENCE AND TECHNOLOGY P.O. BOX 11000, FI-00076 AALTO http://www.aalto.fi

Author Prasantha Reddy Mudimela

Name of the dissertation
CVD synthesis of carbon nanomaterials

Manuscript submitted 24.08.2010	Manuscript revised 25.10.2010
Date of the defence 18.11.2010	
☐ Monograph	☒ Article dissertation (summary + original articles)

Faculty	Faculty of Information and Natural Sciences
Department	Department of Applied Physics
Field of research	Nanotechnology
Opponent(s)	Dr. Nicole Grobert
Supervisor	Professor Esko I. Kauppinen
Instructor	Docent Albert G. Nasibulin

Abstract

This thesis describes the development of methods for the controlled synthesis of carbon nanotubes (CNTs) and carbon nanofibers (CNFs) on flat substrates and on micron sized particles. The carbon nanomaterials were synthesized using three different types of CVD reactors at atmospheric pressure.

The vertical CVD reactor was used to study CNT formation on thermally oxidized silicon wafers and to synthesize individual single-walled CNTs on Si_3N_4 substrates. By using CO as the carbon source and iron as the catalyst, the temperature dependence of CNT growth on the silica substrate was studied by changing the CO_2 concentration and catalyst sputtering time. A variation of the number of CNT walls from 1 to 4 was found by changing the synthesis temperature from 590 to 1070 °C, together with CO_2 concentration. This incremental variation of the number of CNT walls as well as the CNT lengths with temperature was explained by an enhancement of carbon solubility and diffusivity. Individual single-walled CNT synthesis was performed across 1.5 μm wide Si_3N_4 slits for studying the chirality dependent properties of individual tubes.

By employing a horizontal laboratory scale CVD reactor, we reported for the first time the growth of CNFs on cement and clinker particles without additional catalyst. CNFs and CNTs were also synthesized on silica particles impregnated by iron salt. To synthesize CNTs and CNFs on cement particles on a semi-industrial scale, a screw feeder reactor was designed and constructed to provide a continuous feed of the particles. FT-IR measurements and XRD characterization revealed that no major changes were found in the crystallinity of cement at optimized synthesis temperatures below 750 °C. This allowed us to get a good dispersion of the carbon nanomaterials in a cement matrix to improve the properties of composites. The compressive strength and electrical conductivity measurements using this novel cement hybrid material (CHM) revealed a 2-fold increase in the compressive strength and 40-fold increase in the electrical conductivity after 28 days curing in water.

Keywords Carbon nanotubes, carbon nanofibers, cement, temperature, silica particles

ISBN (printed) 978-952-60-3454-6	ISSN (printed) 1795-2239
ISBN (pdf) 978-952-60-3455-3	ISSN (pdf) 1795-4584
Language English	Number of pages 69 p. + app. 54 p.
Publisher Aalto University School of Science and Technology	
Print distribution Department of Applied Physics, Aalto University School of Science and Technology	
☒ The dissertation can be read at http://lib.tkk.fi/Diss/2010/isbn9789526034553/	

Preface

The research work was carried out at Nanomaterials Group, Department of Applied Physics, Aalto University School of Science and Technology. My sincere gratitude goes to Professor Esko I. Kauppinen for giving the opportunity to pursue doctoral studies at his group. His mentorship and valuable suggestions were very useful during the course of the work.

The thesis would not be possible without the guidance and support from Docent Albert G. Nasibulin in all stages of the work. I am grateful to all my co-authors especially Dr. Hua Jiang, Dr. Sergey Shadakov, Dr. Andrzej Cwirzen, Dr. Markus Valkeapää, Larisa Nasibulina, Dr. Andreas Johansson and Professor Mika Pettersson.

I also would like to thank the whole former and present personnel of the Nanomaterials Group including Dr. Janne Raula, Dr. Ilya Anoksin, Dr. He Maoshuai, Dr. Anna Lähde, Dr. Virginia Ruiz, Toma Susi, Ying Tian, Delphine Chassaing, Simas Rackauskas, Antti Kaskela, Kimmo Mustonen, Zhen Zhu, Marina Timmermans and Maryam Borghei for their support during the research work. A special thanks goes to Dr. Anton Anisimov for his co-operation during the laboratory work and for teaching a bit Russian.

I appreciate Jayanta Sarkar for his help during the work and fruitful discussions. I am thankful to the people at VTT, mainly Professor Jorma K. Jokiniemi, Dr. Unto Tapper, Raoul Järvinen and Teemu Kärkelä for their help as well to use SEM. Also friends and colleagues at Low Temperature Laboratory, Nanotechnology and Electron Physics

Groups of Aalto University are acknowledged for their help in practical work related problems.

Furthermore, I would like to thank the pre-examiners of my thesis, Professor Markku Leskelä and Docent Krisztián Kordás, for their invaluable feedback and useful comments.

Though I came from electronics and communication engineering background, the research work during the PhD studies gave me the pleasure and struggle of learning various multidisciplinary subjects ranging from carbon nanotube/nanofiber synthesis, cement chemistry, iron oxide needle synthesis, sensor measurements to clean room work exposure. Even though sensor results are not included in the work, I am thankful to Dr. Paula Heikkilä and Dr. Kestutis Grigoras for their help in clean room. I appreciate Aapo Varpula for his help during sensor measurements. I would like to acknowledge Dr. Vladimir Ermolov and Nokia Corporation for the support in sensor project. The freedom of learning these multidisciplinary research fields was possible due to the generous funding from National Doctoral Programme for Nanoscience (NGS-NANO) (formerly known as National Graduate School in Nanoscience). I am indebted to NGS-NANO.

I would like to thank all of my friends here in Finland with whom I have had so many memorable moments and also my friends from India who are supporting me in all phases of my life. I am grateful to the people who taught me the multidisciplinary subjects of nanoscience and technology. I thank my parents and my brother, Ashok

Mudimela, for their unconditional support. I thank my wife, Supraja Guda, for her affection and understanding the nature of my work.

Espoo, October 2010

Prasantha R. Mudimela

Contents

Preface **5**

Contents **8**

List of Publications **10**

List of Symbols and Abbreviations **13**

1 Introduction **15**

1.1 Aim of the thesis 17

2 Literature review **19**

2.1 Carbon nanostructure properties and applications 19

2.2 Synthesis methods 23

3 Experimental **27**

3.1 Characterization methods 27

3.2 Synthesis methods 28

3.2.1 Vertical CVD reactor 28

3.2.2 Horizontal CVD reactor 30

3.2.3 Screw feeder reactor 32

4 Results and Discussion **34**

4.1 CNT synthesis on substrate in vertical CVD reactor 34

4.2 CNT/CNF synthesis on particles 46

4.2.1 Synthesis in horizontal CVD reactor 46

4.2.2 Synthesis in screw feeder reactor 50

4.2.3 Application for construction materials 53

5 Conclusions **58**

6 References **60**

APPENDICES

Publications I-V

List of Publications

I **Mudimela**, **P.R.**, Nasibulin, A.G., Jiang, H., Susi, T., Chassaing, D., Kauppinen, E.I., 2009. Incremental variation of the carbon nanotube walls with the growth temperature. *J. Phys. Chem. C*, 113 (6), 2212–2218.

II Nasibulin, A.G., Shandakov, S.D., **Mudimela**, **P.R.**, Kauppinen, E.I., 2010. CNT morphology and structure by CVD method on iron catalyst in the presence of carbon monooxide. *Nanotechnologies in Russia*, 5 (3-4), 198-208.

III Myllyperkiö, P., Herranen, O., Rintala, J., Jiang, H., **Mudimela**, **P.R.**, Zhu, Z., Nasibulin, A.G., Johansson, A., Kauppinen, E.I., Ahlskog, M., Pettersson, M. Femtosecond four-wave-mixing spectroscopy of suspended individual semiconducting single-walled carbon nanotubes. Accepted to be published in *ACS Nano*.

IV **Mudimela**, **P.R.**, Nasibulina, L.I, Nasibulin, A.G., Cwirzen, A., Valkeapää, M., Cwirzen, K.H., Malm, J.E.M., Karppinen, M.J., Penttala, V., Koltsova, T., Tolochko, O.V., Kauppinen, E.I., 2009. Synthesis of carbon nanotubes and nanofibers on silica and cement matrix materials. *J. Nanomater.*, 2009, 52612.

V Nasibulin, A.G., Shandakov, S.D., Nasibulina, L.I., Cwirzen, A., **Mudimela**, **P.R.**, Cwirzen, K.H., Grishin, D.A., Gavrilov, Y.V., Malm, J.E.M., Tapper, U., Tian, Y., Penttala, V., Karppinen, M.J., Kauppinen, E.I., 2009. A novel cement-based hybrid material. *New J. Phys.*, 11, 023013.

Other Contributed Publications

VI Nasibulin, A.G., Rackauskas, S., Jiang, H., Tian, Y., **Mudimela**, **P.R.**, Shandakov, S.D., Nasibulina, L.I., Sainio, J., Kauppinen, E.I., 2009. Simple and rapid synthesis of Alpha-Fe_2O_3 nanowires under ambient conditions. *Nano Res.*, 2 (5), 373-379.

VII Cwirzen, A., Cwirzen, K.H., Nasibulin, A.G., Kaupinen, E.I., **Mudimela**, **P.R.**, Penttala, V., 2009. SEM/AFM studies of cementitious binder modified by MWCNT and nano-sized Fe needles. *Mater. Character.*, 60 (7), 735-740.

VIII Cwirzen, A., Cwirzen, K.H., Penttala, V., Nasibulina, L.I., Shandakov, S.D., **Mudimela**, **P.R.**, Nasibulin, A.G., Kauppinen, E.I. 2009. Properties of high yield synthesized carbon nanofibers / portland cement composite. *Adv. Cem. Res.*, 21 (4), 141-146.

IX Nasibulina, L.I., Anoshkin, I.V., Shandakov, S.D., Nasibulin, A.G., Cwirzen, A., **Mudimela**, **P.R.**, Cwirzen, K.H., Malm, J.E.M., Koltsova, T.S., Tian, Y., Vasilieva, E.S., Penttala, V., Tolochko, O.V., Karppinen, M.J., Kauppinen, E.I., 2010. Direct synthesis of carbon nanofibers on cement particles. *Trans. Res. Rec.*, 2142, 96-101.

X Nasibulina, L.I., **Mudimela**, **P.R.**, Nasibulin, A.G., Koltsova, T.S., Tolochko, O.V., Kauppinen, E.I., 2010. Synthesis of carbon nanotubes and nanofibers on silica and cement particles. *Questions in Material Science* (Voprosy Materialovedeniya), 61(1), 121-126.

XI He, M., Rikkinen, E., Jiang, H., Sainio, J., **Mudimela**, **P.R.**, Nasibulin, A.G., Kauppinen, E.I., Niemelä, M., Krause, A.O.I. Temperature Dependent G-band intensity of Raman Spectra in SWCNTs. Submitted.

Author's contribution

I. The author is mainly responsible for all parts of the work and wrote the manuscript.

II. The author contributed to optimize the CNT synthesis, SEM characterization, sample preparation for TEM and analyzing the results.

III. The author contributed to optimizing individual SWCNT synthesis and SEM characterization.

IV. The author is mainly responsible for all parts of this work (except synthesis on clinker particles) and wrote the manuscript.

V. The author contributed to design and construction of screw feeder reactor, CNT synthesis, SEM characterization and co-writing the paper.

List of Symbols and Abbreviations

σ_{sl}	surface tension between liquid and solid
ΔH_{fus}	latent heat of fusion
C	graphitized carbon
C_h	length of chiral vector
d	diameter
G	gypsum
r	radius
T_o	bulk melting temperature
T_m	melting temperature
V	volume of a metal atom
Ar	argon
C_2H_2	acetylene
CaO	free lime, calcium oxide
$CaSO_4 \cdot 2H_2O$	gypsum
Ca_2SiO_4	dicalcium silicate
$Ca_3Al_2O_6$	tricalcium aluminate
Ca_3SiO_5	alite
CH_4	methane
CO	carbon monoxide
CO_2	carbon dioxide
N_2	nitrogen
CHM	cement hybrid material
CNF	carbon nanofiber
CNT	carbon nanotube
CVD	chemical vapor deposition
DWCNT	double-walled carbon nanotube
FT-IR	Fourier-transform infrared
MWCNT	multiwalled carbon nanotube
RBM	radial breathing mode
SEM	scanning electron microscope
SR	sulfate resistant
SWCNT	single-walled carbon nanotube
TEM	transmission electron microscope
TGA	thermogravimetric analysis
XRD	x-ray diffraction

1 Introduction

Carbon can exist in several allotropes and forms such as diamond, graphite, fibers, fullerenes and nanotubes. Diamond and graphite have been well known carbon material for centuries. Carbon filaments, presumably nanotubes, were first observed by Radushkevich and Lukyanovich in 1952 [1]. Hillert and Lange [2] reported the concentric and bamboo textures of carbon filaments in 1958. Bollmann and Spreadborough [3] synthesized a roll of graphite sheet in 1960. Oberlin et al. [4] reported the chemical vapour deposition (CVD) growth of carbon nanofibers (CNFs) by benzene decomposition. Fullerenes were discovered by Kroto et al. in 1985 [5]. In 1991, Iijima reported double-walled carbon nanotubes (DWCNTs) and multiwalled carbon nanotubes (MWCNTs) [6] and explained their crystal structure. His remarkable findings caused the scientific community to focus into nanotube research. Two years later SWCNTs were independently synthesized by Iijima and Ichihashi [7] and Bethune et al. [8] with the help of metal catalyst particles. Nowadays, CNTs attract significant attention in the scientific community because of their remarkable optical, electronic, thermal, mechanical and chemical characteristics. Based on these properties a large variety of interesting and important applications has been suggested.

Arc discharge, laser ablation and CVD methods are the most commonly used techniques for the synthesis of the CNTs. Arc discharge and laser ablation are based on the condensation of carbon atoms generated from the evaporation of solid carbon sources at high temperatures. Neither of these methods provide the possibility of patterning the catalyst for controlling the CNT placement, e.g. on a chip. The CNTs grown by these

methods are highly tangled, with unwanted carbon and metal impurities, which make them difficult to purify, manipulate, and assemble for practical applications.

CVD is based on the process where a carbon precursor is transported via the vapour phase to the reaction chamber where it decomposes on the surface of the catalyst particles. The CVD method allows CNT growth at much lower temperatures compared to the arc discharge and laser ablation methods. The CVD method is a controllable process for the selective synthesis of CNTs either individually or in bulk. As a carbon source, usually hydrocarbons (C_2H_2, CH_4, C_2H_4, etc.) or CO are used. Hydrocarbon decomposition has the drawback of forming an amorphous carbon coating, due to the self-pyrolysis of the reactant at high temperatures, which generally requires additional purification steps prior to CNT utilization. This can be avoided by using CO, which disproportionates only on the catalyst surface.

The CVD synthesis can be carried out either in the gas phase or on substrate materials. The CVD process realized in the gas phase is called a floating catalyst or an aerosol CVD method. CNT growth on the supported materials has several advantages over other methods. Usually no sonication and oxidative purification are involved for the SWCNT samples grown directly on the device substrate, which significantly reduces the possibility of defect formation and altering of the CNT properties. Patterns can be introduced by various lithography methods, which is useful for many applications such as field emission, sensors, transistors, memory devices etc. The substrate materials used for the synthesis can be divided into particles and flat substrates. For growth on particles, SiO_2, MgO and Al_2O_3 are the most commonly used substrate materials with

both hydrocarbons [9-11] and CO [12-14]. Zeolites [15] and $CaCO_3$ [16] are also known to provide good substrates for the CNT growth.

In case of flat substrates, Kong et al. [17] synthesized SWCNTs from patterned iron catalytic islands on a SiO_2 substrate using methane as a carbon. Huang et al. [18] synthesized millimetre long SWCNTs with iron catalyst on a SiO_2 wafer using CO. Zheng et al. [19] reported that the addition of H_2 greatly enhanced the SWCNT growth using iron catalyst on a silica substrate by CO disproportionation. Peng et al. [20] and Kasumov et al. [21] synthesized SWCNTs from iron catalyst on Si_3N_4 membranes using CH_4 and C_2H_2, respectively. CNT syntheses on Al_2O_3 substrates have been extensively described using hydrocarbons [22, 23] and CO [19] as carbon sources. Other materials, including quartz [24], sapphire [25], diamond [26] and mica [27] were also efficiently used as supports for CNT growth.

1.1 Aim of the thesis

Despite the great progress in the synthesis of CNTs, the growth mechanism is not fully known yet. Understanding of the CNT formation is crucial to achieve efficient control over the CNT structure and yield. One of the main goals of this work is to investigate the growth of CNTs on flat substrates and therefore to enable the control of their properties. For this purpose we have developed a vertical CVD reactor with well controlled CO flow conditions. Variation in the experimental conditions such as catalyst sputtering time, CO_2 concentration and the synthesis temperature have allowed us to control the length, diameter and number of CNT walls (Publications I, II). Moreover,

careful control of the flow conditions has enabled us to synthesize individual SWCNTs across 1.5 μm wide slits for studying the chirality dependent properties of individual tubes (Publication III).

The knowledge and experience obtained during the investigation of CNTs on the flat substrates were essential to grow carbon nanomaterials on the surface of particles like cement and clinker. Significantly, these particles, probably the most important construction components, naturally contain the iron catalyst needed, but have never before been utilized for the growth of CNFs/CNTs. To examine our concept concerning the possibility of CNT/CNF growth on cement and clinker particles without additional catalysts we built and utilised a simple horizontal fixed powder bed CVD reactor (Publication IV). To enhance the production rate of the carbon nanomaterials we designed and constructed a semi-industrial scale screw feeder reactor, with a continuous particle feed. Optimization of the growth conditions has allowed us to synthesize cement hybrid materials (CHMs) with different concentrations of CNFs. The possibility to grow CNFs on these construction materials allowed us to get a good dispersion of the nanomaterial in the cement matrix and therefore to significantly improve the physical properties of the hardened cement paste. The CHM has been proven to increase by 2-fold the compressive strength and by 40-fold the electrical conductivity of the hardened paste. To the best of our knowledge, these significant compressive strength and electrical conductivity enhancements with the help of CNTs and CNFs are the highest reported (Publication V).

2 Literature review

2.1 Carbon nanostructure properties and applications

SWCNTs form a hexagonal network of carbon atoms rolled into a seamless, hollow cylinder, with each end capped with half a fullerene molecule [28]. Rolling of the graphene sheet at different angles creates a visible twist or spiral in the molecular structure, giving it chiral properties. The basic structure of a SWCNT is specified by a single vector called the chiral vector Ch. As shown in Figure 1, this vector is denoted by OA and is the section of the nanotube perpendicular to the nanotube axis, which when rolled up is the circumference of the tube. Figure 1 shows the unrolled lattice of the nanotube and, in this case, the direction of the nanotube axis is given by the vector OB. The lattice can then be rolled to form a cylinder by lining up the points so that O is on top of A and B is on top of B'.

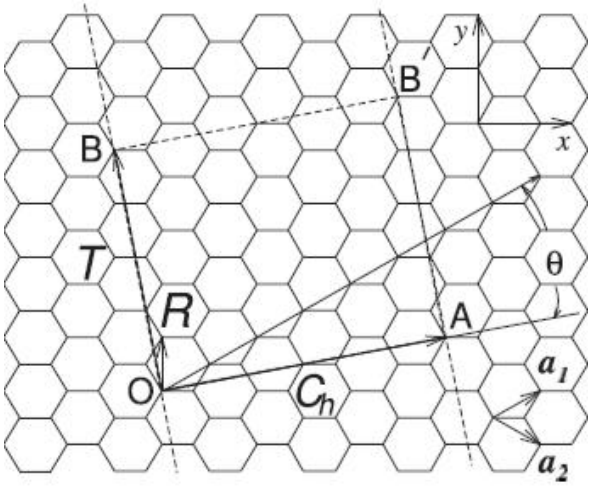

Figure 1. Chirality in nanotubes [28]

The chiral vector Ch is then determined by the real space lattice vectors a_1 and a_2, which are also defined in Figure 1. This leads to the following equation:

$$C_h = na_1 + ma_2 \equiv (n, m). \quad (1)$$

A nanotube is then specified by the pair of the integers (n, m), where $0 \leq m \leq n$.

For CNTs the parameter 'a' (~ 2.49 Å) is the length of the unit vectors. The length of the chiral vector is

$$|C_h| = a\,(n^2 + m^2 + nm)^{1/2} \quad (2)$$

and thus the diameter of the SWCNT is

$$d = |C_h|/\pi. \quad (3)$$

The chiral angle obtained as

$$\theta = \arctan\,(\sqrt{3}m/\,(2n + m)). \quad (4)$$

The main symmetry classification of the tube defines it as being either achiral or chiral. An achiral tube is defined as one where the mirror image of the tube is identical to the original one. A chiral tube is then defined as a tube where the mirror image cannot be superposed on to the original tube; it shows spiral symmetry. There are two types of achiral tubes, which are known as armchair and zigzag nanotubes. These two types can be seen in Figure 2 where (a) is an armchair tube and (b) is a zigzag tube. These two tubes get their names from the shape of the cross-sectional ring at the circumference of the nanotubes. An armchair nanotube is then defined as the case where n = m ($\theta = 30°$) in equation 1, and a zigzag corresponds to the case where m = 0 ($\theta = 0°$). All other chiral vectors ($0 < \theta < 30°$) correspond to the production of chiral nanotubes (Figure 2c). Those indices uniquely determine whether the SWCNT is metallic or semiconducting: when $|m - n| = 3k$ (k is an integer), the tube is metallic but if $|m - n| = 3k \pm 1$, the tube is semiconducting.

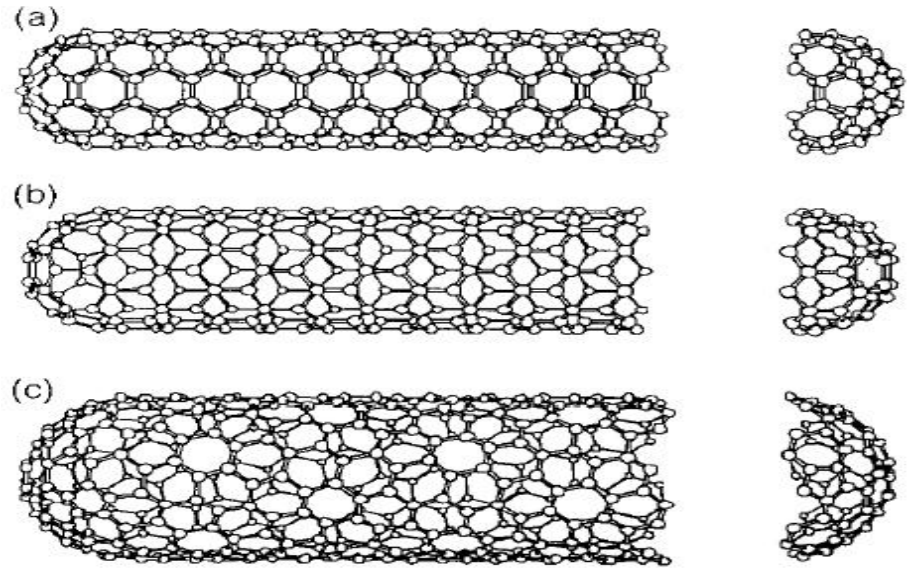

Figure 2. Three different structures of SWCNTs: (a) armchair, (b) zigzag and (c) chiral [29].

CNTs can also be found in other forms, for example the DWCNT (Figure 3b) and MWCNT (Figure 3a, c). DWCNT and MWCNT contain 2 and more coaxial cylinders, respectively, with each cylinder being a SWCNT with weak van der Waal forces binding the cylinders together. The physical properties of carbon nanotubes are shown in table 1.

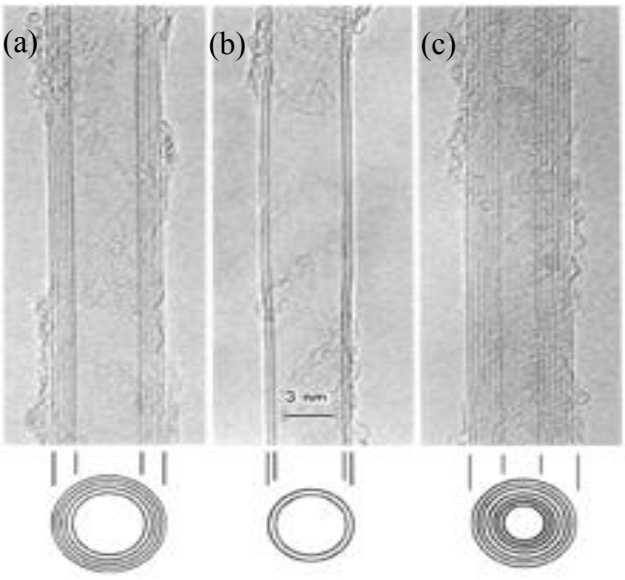

Figure 3. (a) and (c) MWCNTs (b) DWCNT [6]

Table 1. Physical properties of carbon nanotubes [30]

Mechanical properties	
Young's modulus of MWCNTs	~1000-1200 GPa
Young's modulus of SWCNT ropes	~1000 GPa
Tensile strength SWCNT ropes	~60 GPa
Electrical Properties	
Resistivity of SWCNTs and MWCNTs	10^{-6} Ω m
Maximum current density of SWCNTs and MWCNTs	10^{7}-10^{9} A/cm^2
Quantized conductance of MWCNTs (Theoretical/measured)	(6.5 kΩ)$^{-1}$ / (12.9 kΩ)$^{-1}$
Thermal properties	
Thermal conductivity of SWCNTs	1750-5800 W/(mK)
Thermal conductivity of MWCNTs	>3000 W/(mK)

A carbon nanofiber (CNF) is characterized by a graphitic like structure with variable alignments of laminated hexagon layers along the fiber axis [31]. The graphitic platelet sheets that make up the nanofiber can be mainly divided into three different configurations, as shown in Figure 4. In the tubular form, graphitic walls are parallel to the fiber axis (Figure 4a) and this is a MWCNT. Figure 4b shows that the graphitic layers are at an angle to the fiber axis and this is usually called the herringbone (fish bone) or cup stacked structure due to its shape. In the final configuration, graphitic layers are positioned perpendicular to the fiber axis and are stacked on top of each other (Figure 4c).

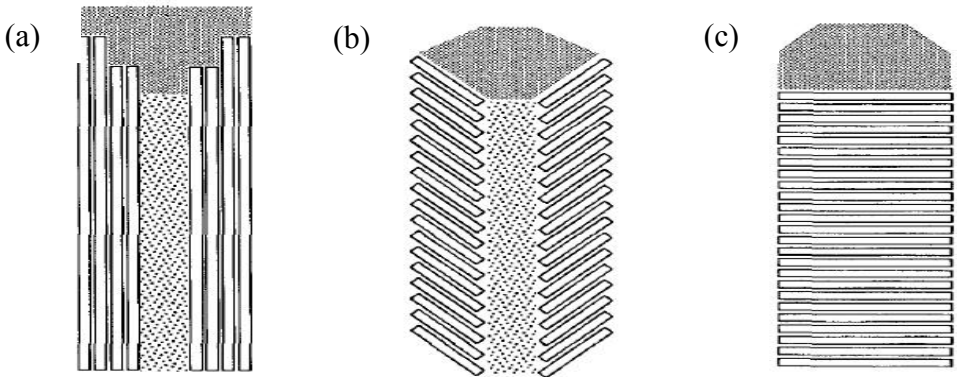

Figure 4. Schematic representation of various arrangements of graphitic platelets in carbon nanofibers (a) tubular, (b) at angle (c) perpendicular to the fiber axis [32].

Table 2. Physical properties of carbon nanofibers [33]

Properties	Value
Tensile strength	2.7 GPa
Tensile modulus	400 GPa
Ultimate strain	1.5%
Density	1.8 g/cm^3
Electrical resistivity	10^{-5} Ω m
Thermal conductivity	20 W/(mK)

Due to their remarkable properties, CNTs have been investigated for various applications such as light emitting diodes [34], sensors [35], actuators [36], logic circuits [37], super capacitors [38], filters [39] and ceramic and reinforced composites [40, 41]. CNFs are used in fuel cells [42], supercapacitors [43] sensors [44, 45] and tissue engineering [46] and composite applications [47].

2.2 Synthesis methods

The most familiar methods for the nanotube synthesis are arc discharge, laser ablation and CVD.

Arc discharge method. A schematic view of the arc discharge method is given in Figure 5. A potential difference of 20 - 30 V is applied between two graphite rods placed in a noble gas flushed reaction chamber at a constant pressure of 200 to 500 Torr [48, 49]. The graphite electrodes are moved close to each other until a plasma is produced, usually at a distance of approximately 1 mm or less. MWCNTs are produced when pure graphite electrodes are used. In case of SWCNT synthesis, the anode graphite is doped with metal catalyst.

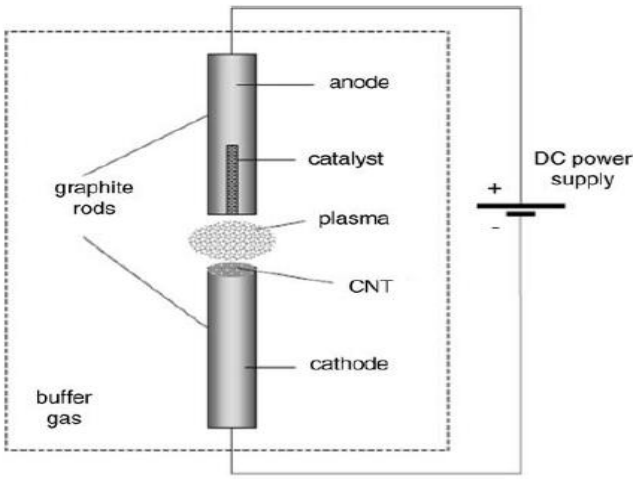

Figure 5. Schematic diagram of arc-discharge [50]

Laser ablation method. In this method, a pulsed laser vaporizes a metal-graphite composite in a reactor which is at high temperature. To get uniform vaporization, a laser beam scans the target surface. Once the vacuum is established in a tube shaped reactor, it is filled with argon to sweep the carbon soot produced by laser vaporization from the high temperature zone to the water cooled copper collector. The initial laser vaporization pulse is followed by a second pulse for more uniform vaporization, which minimizes the amount of carbon deposited as soot. Carbon clusters from the graphite target are cooled and condensed on the copper collector. Laser ablation method was initially developed for the synthesis of fullerenes by Kroto et al. [5]. This method was utilised for the formation of CNTs by the use of catalyst in carbon target [51]. A schematic view of the laser ablation setup is shown below.

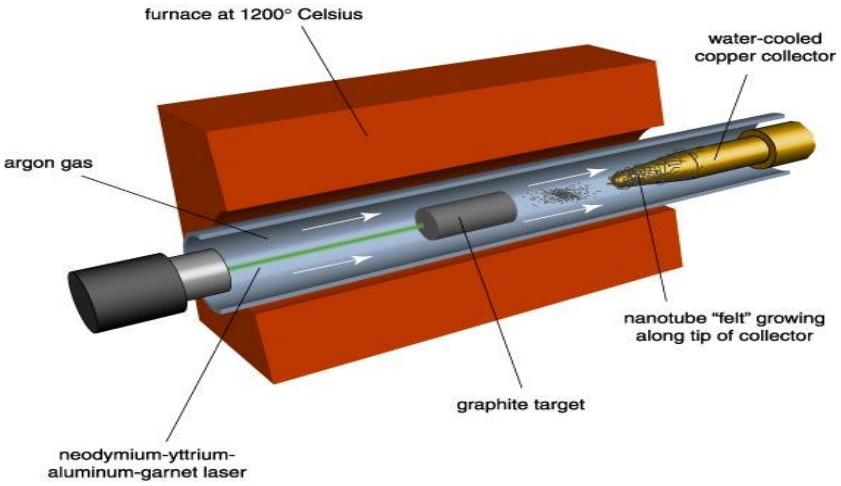

Figure 6. Schematic diagram of laser ablation technique [51]

Chemical vapour deposition. In principle, chemical vapor deposition can be understood as a chemical process in which volatile precursors are used to provide a carbon feed source to a catalyst particle at elevated temperatures (350–1000 °C) [50]. Chemical vapour deposition is the term used to describe heterogeneous reactions in which both solid and volatile products are formed from a volatile precursor through chemical reactions, and the solid products are deposited on a substrate. Metals are used to catalyze CNT growth. Usually, transition metals, in particular iron, cobalt and nickel are used as catalysts because of their high carbon solubility into these metals [52]. Apart from metal catalysts, CNTs were also successfully synthesized on metal free catalyst materials such as zirconia nanoparticles [53], SiGe islands [54] and sputtered SiO_2 film [55]. The advantage of the CVD method is that it allows control over the morphology and structure of the CNTs produced. Both MWNT and SWCNT syntheses have been well developed. This method can be applied to the industrial production of CNTs in the form of powder and forests [56-58]. In addition, one can synthesize well-separated individual CNTs, supported either on flat substrates or suspended across slits. The

CNTs synthesized with the CVD method can be directly used to fabricate components for nanoscale electronics.

The CVD process realized in the gas phase is called the aerosol CVD method. Various studies of the aerosol synthesis of CNFs [59, 60], MWCNTs [61, 62] and SWCNTs [63, 64] have already been reported. Aerosol methods hold out the promise for large-scale production as this method allows continuous feeding of the carbon precursor and catalyst particles into the system. These methods may potentially permit control of the catalyst particle size, offer continuous processing and provide high product purity.

3 Experimental

3.1 Characterization methods

A Leo Gemini DSM982 SEM was used to examine the length and density of the synthesized CNTs and CNFs on the substrate material surface (Publications I-V). The morphology and structure of the synthesized CNF and CNTs (Publications I-V) were characterized by using a Philips CM200-FEG TEM equipped with a Gatan 794 multi scan charge-coupled device (CCD) camera for digital data recording. TEM was also used for characterising the SWCNTs by their diffraction patterns [Publication IV]. A GASMET DX4000 (Temes Instruments) Fourier-transform infrared spectroscopy (FT-IR) was employed to study the gas products coming out of the vertical and horizontal CVD reactors (Publications I, IV). Raman spectroscopy with a Nd:YAG green laser (532.25 nm, 30 mW) was employed to characterize the individual SWCNTs grown across the slits (Publication III) and also used for characterizing CNFs/CNTs grown on cement (Publication V).

To determine possible changes in the cement after high temperature treatment, XRD analysis was carried out with Philips PW 1820 (Publication IV) and Bruker D8 Advance (Publication V) X-ray diffractometers using CuKα radiation. To estimate the carbon nanomaterial yield on the treated cement particles, thermogravimetric analyses (TGA) were performed using a Netzsch STA 449 C thermobalance. SEM-EDX mapping was used for elemental mapping of the cement paste to check the dispersion of CNTs/CNFs (Publication V).

3.2 Synthesis methods

3.2.1 Vertical CVD reactor

In order to investigate the formation of CNTs on flat substrates, we designed a vertical CVD reactor with well controlled gas flow conditions. The reactor was built in the vertical orientation to maintain laminar conditions and to avoid recirculation inside [65]. This allowed us to synthesize CNTs along the direction of the gas flow.

Thermally oxidized silicon wafer and Si_3N_4 were utilized as substrates. Investigations of the CNT growth mechanism were carried out on 300 nm SiO_2 on Si wafer substrates in the temperature range from 550 to 1120 °C. This reactor was used to grow individual SWCNTs across 200 nm thick Si_3N_4 slits with a width of 1.5 μm to study the chirality dependent properties.

Iron catalyst was sputtered on the substrate using an Agar sputter coater (model 108A) under 0.05 mbar Ar pressure at 20 mA DC current. In the experiments with oxidized silicon wafers, the sputtering time for iron was varied from 5 to 20 s. In the case of the Si_3N_4 substrate, the sputtering time for nickel was maintained at 6 s.

The vertical CVD reactor consisted of a ceramic tube with an inner diameter of 2.2 cm placed inside a 44 cm long furnace, as shown in Figure 7. For CNT growth, the reactor was first heated to the desired temperature in a flow of Ar (400 cm^3/min). A piece of a silica wafer (about 1x1 cm^2) with deposited iron catalyst was attached to the stainless steel rod (sample holder) and then inserted into the middle of the reactor. A thermocouple was placed inside the rod to monitor the temperature of CNT growth.

Then, a H_2 flow (200 cm^3/min) was introduced into the reactor for the duration of the synthesis. After 5 min, the Ar flow was replaced by CO with the same flow rate. After 30 min growth time, the H_2 was switched off, the CO flow was again replaced by Ar and the rod was pulled to the dilutor, which was used for cooling the substrate to a temperature below 100 °C. The reduction and growth periods were kept constant for most of the experiments, unless otherwise specified. The dilutor was a porous tube, through which a 12 l/min room temperature N_2 flow was introduced. Depending on the synthesis conditions, the mole fraction of CO_2 added into the reactor was varied from 0 to 38.7%. The experiments were carried out under atmospheric pressure in the temperature range from 590 to 1120 °C.

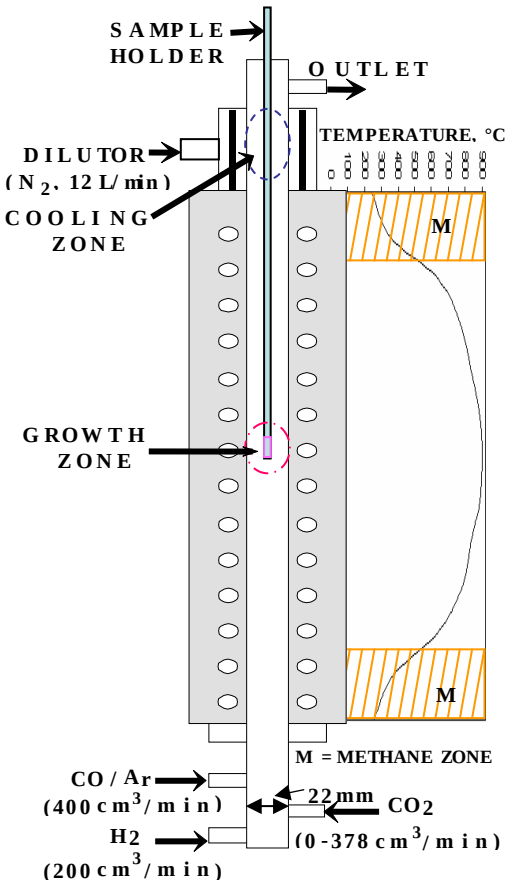

Figure 7. Schematic representation of the CVD reactor along with a temperature profile at 900 °C. (Publications I, II)

For TEM observations, CNTs were directly grown on SiO_2/SiO Ni TEM grids (SPI, USA). For individual CNT synthesis, Si_3N_4 was chosen due to its high dielectric constant, strong resistance to impurity diffusion and compatibility with conventional CMOS technology. For the CNT synthesis, nickel sputtered Si_3N_4 slits were fixed in the direction of gas flow in such a way that the CNTs grew across the slit. The growth was maintained at a temperature of 740 °C. The same gas concentration was used as mentioned above with 12 cm^3/min CO_2 flow for a period of 20 minutes.

3.2.2 Horizontal CVD reactor

A horizontal reactor was built to examine the possibility of CNT/CNF growth on the surface of cement and clinker. Cement (clinker + gypsum) is the main constituent of concrete and therefore very important in the construction industry. The growth of carbon nanomaterials was also examined on the surface of a model material, namely silica fume particles impregnated by iron salt. Silica particles are also known to be used in the construction industry to increase the strength of concrete by acting as a microfiller and as a reactant in the pozzolanic reaction during cement hydration [66].

The horizontal CVD reactor consists of a 40 cm long quartz tube with inner diameter of 1.2 cm placed inside 25 cm long furnace. A schematic view of the horizontal reactor is shown in Figure 8. C_2H_2 and CH_4 were utilized as carbon sources and H_2 was used as the reducing agent. The number mean size of the silica particles was varied from 100 nm to 2 μm. For impregnation of catalyst, 2 g of silica particles was mixed with 150 ml aqueous iron nitrate (3.8×10^{-3} M) solution. Then, the solution was stirred for 1 h and dried in an oven at 90 °C. The obtained powder was ground before placing in the

reactor. For this study, sulphate-resistant Portland type cement (CEM I 42.5N) with 3.4% (weight) Fe_2O_3 produced by Finnsementti Oy was used. The number mean size of the cement particles varied from 1 to 20 µm and the powder was directly employed for the CNT/CNF growth. In order to permeate the cement with catalyst, 0.4 g of cement was added to 56 ml ethanol based iron nitrate (3.8×10^{-3} M) solution. The solution was stirred for 1.5 hours and dried under ambient conditions.

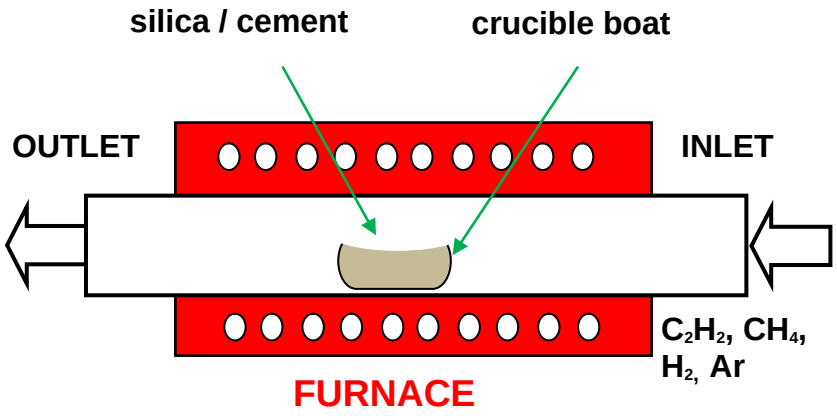

Figure 8. Schematic view of the horizontal CVD reactor (Publication IV)

For CNT/CNF synthesis, impregnated silica powder were placed in a crucible boat, introduced into the reactor, and heated to the synthesis temperature in an Ar atmosphere at a flow rate of 280 cm^3/min. In order to reduce iron oxide, Ar was replaced by H_2 with the same flow rate. After 5 minutes C_2H_2, with a flow rate of 28 cm^3/min, was passed through the reactor for 20 minutes. After the synthesis, the C_2H_2 flow was switched off. H_2 was replaced with Ar and the reactor was cooled down to room temperature. In the case of CNF grown on pristine cement and impregnated cement particles, C_2H_2 with same flow rate of 28 cm^3/min was used with the synthesis condition stated above. About 180 mg of cement was coated in an hour. The same procedure was followed for CNF

growth on clinker particles. For the growth on silica particles, experiments were carried out over the temperature range from 550 to 750 °C and the cement treatment was varied from 550 to 900 °C.

3.2.3 Screw feeder reactor

In order to carry out mechanical tests of these materials for construction applications, the amount of the product must be significantly increased. For this purpose, we designed and constructed a novel CVD reactor based on a continuous feeding of the catalyst particles using a screw feeder.

The screw feeder reactor is schematically presented in Figure 9. It consists of a quartz tube (with an internal diameter of 34 mm and a length of 100 cm) inserted in a resistively heated furnace (with a heated length of 60 cm), a cement powder feeder with an adjustable mass feeding rate, a copper screw feeder, a powder collector, and a water cooling system to keep the ends of the tube at room temperature. The overall assembly was named the screw feeder reactor.

For the high yield synthesis of CNTs and CNFs, two types of cement with different concentrations of iron oxide, i.e. Portland sulfate resistant (SR) (4 wt%) and White (0.33 wt%) cements were examined (Table 3). C_2H_2 (with a flow rate of 660 or 860 cm^3/min) was used as the main precursor. To enhance the yield, carbon monoxide (50 or 177 cm^3/min) and carbon dioxide (660 cm^3/min) were added as promoting additives. The residence time of the cement particles in the high temperature reactor zone was regulated by the motor rotation speed, which was varied from 1 to 4 min^{-1},

corresponding to 40 and 10 min residence time, respectively. The experimental investigations were carried out with a powder feed rate of 30 g/hour and a reactor wall temperature range of 400-700 °C.

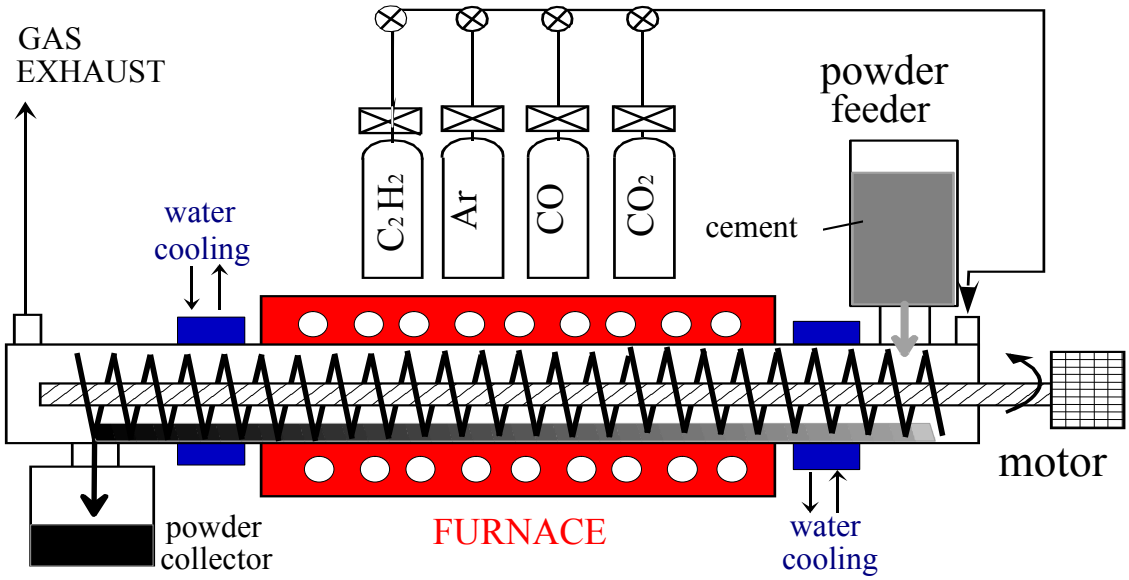

Figure 9. Schematic representation of the experimental setup based on continuous feeding of cement particles using a screw feeder. (Publication V)

Table 3. Oxide content (wt.%) of the Portland cements utilized for CNT/CNF growth.

Oxides / Cement type	CaO	SiO_2	SO_3	Fe_2O_3	Al_2O_3	MgO	K_2O	Na_2O
SR cement	63.1	20.2	3.00	4.0	2.2	2.0	0.31	0.48
White cement	68.7	25.2	2.17	0.33	2.1	0.56	0.06	0.18

4 Results and Discussion

4.1 CNT synthesis on substrate in vertical CVD reactor

In order to investigate the effect of the Fe concentration on CNT morphology, the sputtering time of the catalyst material was varied from 5 to 20 s. For the current examination, the reactor temperature was fixed at 900 ºC. The mole fraction of the introduced CO_2 was kept at 0.7%, which corresponded to the 4 cm^3/min flow rate. The density of CNTs was increased with increase in the sputter time from 5 to 15 s (Figure 10 a, b, c). Further increase in the sputter time decreased the amount of CNTs (Figure 10d). This is probably due to excessive aggregation of catalyst particles, which is not favorable for CNT nucleation and growth.

At higher temperatures, the mobility and, subsequently, the collision rate of catalyst particles on the substrate surface is significantly enhanced. To avoid this at high temperatures, i.e. at 970 °C and 1070 °C, the growth of CNTs was found to be optimum with sputtering times of 11 and 7 s, respectively. For all further experiments at 900 °C and below, a 15 s sputtering time was used unless otherwise specified.

The effect of CO_2 concentration on CNT density was examined at different temperatures. Without added CO_2, the density of the CNTs produced was significantly smaller (Figure 11a). Increasing the CO_2 mole fraction up to 1.32% (8 cm^3/min) resulted in a regular increase of the CNT density (Figure 11b). Further increase in CO_2 concentration led to a decrease in the amount of synthesized CNTs (Figure 11c). No CNTs were found on the substrate at a mole fraction of 2.75% (Figure 11d). Therefore,

1.32% CO_2 concentration was chosen for optimal CNT growth at 900 °C. For optimal CNT synthesis at higher temperatures of 970, 1070 and 1120 °C the CO_2 mole fractions were found to respectively decrease to 0.25, 0.083 and 0.075%. At lower temperatures, from 740 to 590 °C, the optimum concentration increased and varied respectively from 2.0 to 38.7%.

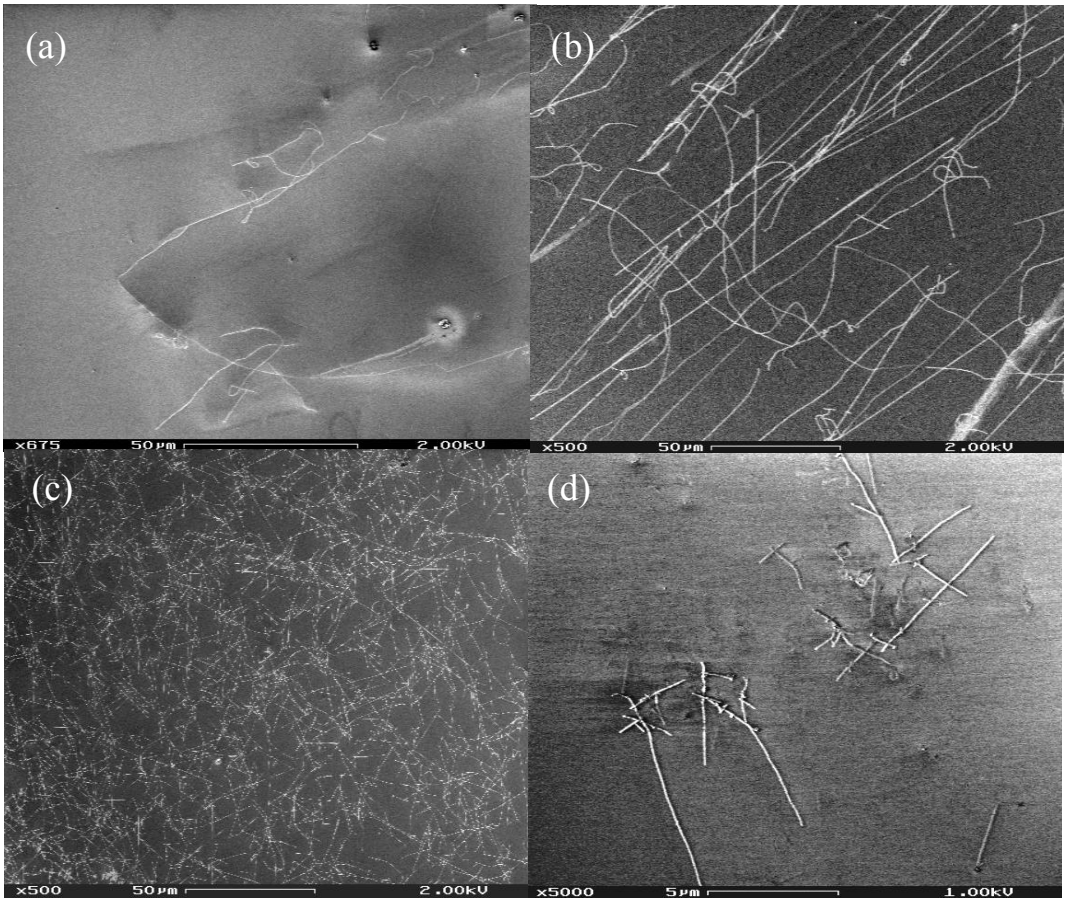

Figure 10. SEM images of CNTs synthesized at 900 ºC with CO_2 concentration of 0.7% showing the effect of sputtering time on the density: a) 5 s; b) 10 s; c) 15 s; d) 20 s. (Publications I, II)

During the TEM observation only single-walled CNTs were found at 590 °C (Figure 12a). TEM characterization of the samples produced at 740 °C revealed predominant single-walled CNT formation. An observation of 25 tubes found that only 2 tubes were double-walled. Mainly (27 of 32 tubes) double-walled CNTs along with a few single-

walled CNTs were synthesized at 900 °C. A typical TEM image of a double-walled CNT is shown in Figure 12b. At 970 °C, 10 triple-walled, 6 double-walled, 3 quadruple-walled and 1 single-walled CNT were found. A typical TEM image of a triple-walled CNT is shown in Figure 12c. At 1070 °C, mainly quadruple-walled CNTs were found (Figure 12d); however, a few CNTs with three and five walls were also detected under these conditions. Increasing the synthesis temperature increased the lengths of CNTs. The variation in length and diameter of CNTs synthesized at different temperatures are shown in Table 4.

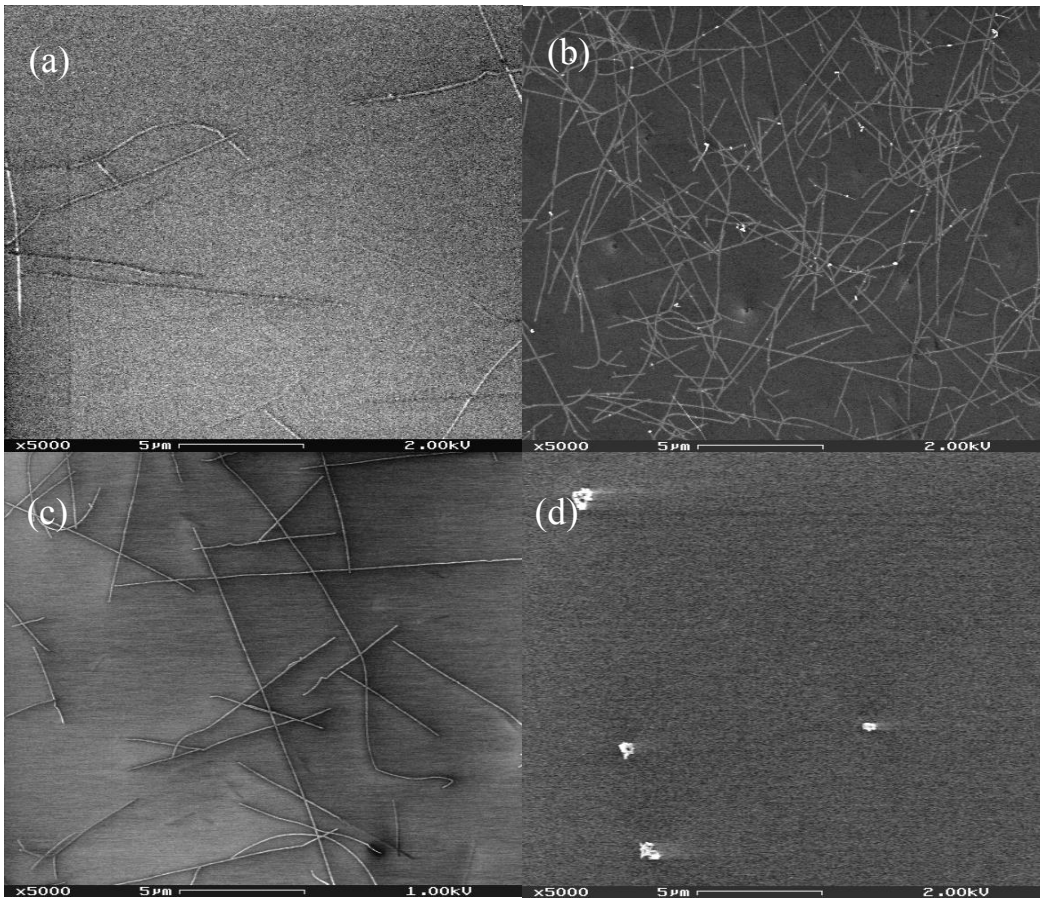

Figure 11. SEM images of CNTs synthesized at 900 °C with sputtering time of 15 s showing the effect of CO_2 mole fraction on the CNT growth: a) 0%; b) 1.32%; c) 2.12%; d) 2.75%. (Publications I, II)

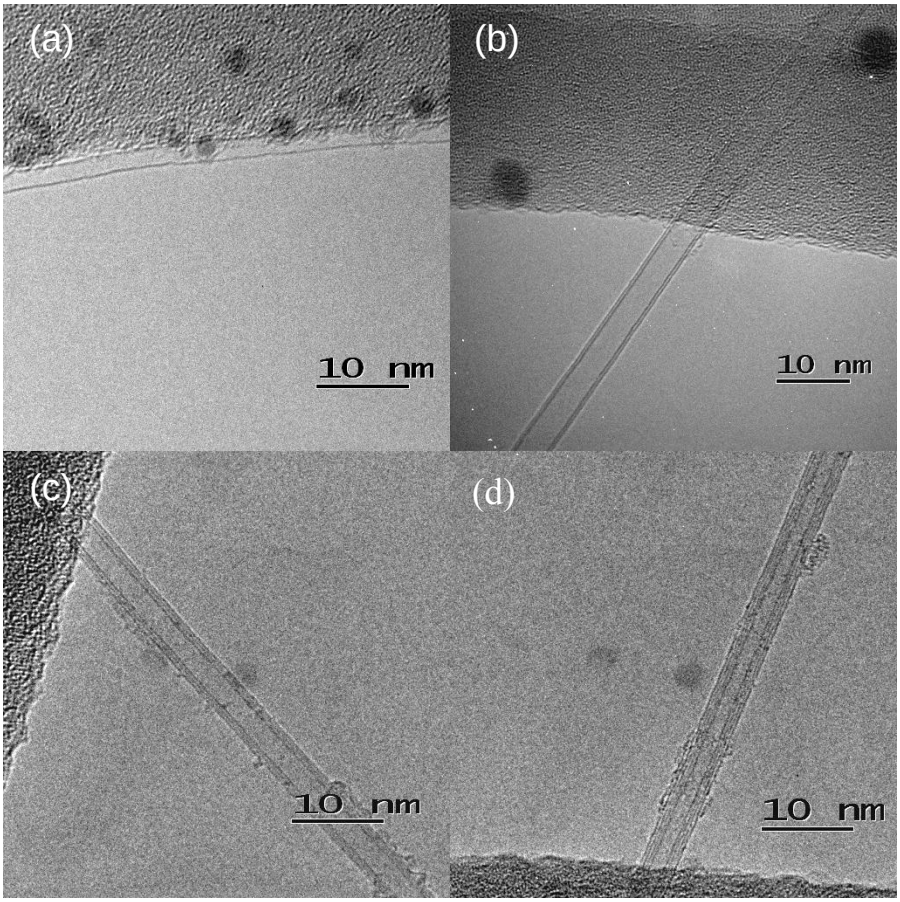

Figure 12. TEM images of typical products synthesized at different temperatures: a) a single-walled CNT at 590 °C; b) a double-walled CNT at 900 °C; c) a triple-walled CNT at 970 °C; d) quadruple-walled CNTs at 1070 °C. (Publications I, II)

Table 4. Variation of the number of walls, diameters and lengths of CNTs produced at different conditions.

Temperature, °C	CO_2 concentration,%	Product, number of walls	CNT diameter, nm	Variation in length, μm
590	38.7	1	2.1 – 2.4	> 2
740	2.00	1,2	1.4 – 2.5	0.5 – 25
900	1.32	2,1	3.6 – 8.4	2 – 100
970	0.25	3,2	3.7 – 7.3	2 – 200
1070	0.083	4,3,2	4.5 – 12	> 350

In order to examine the effect of the catalyst particle diameter on the number of walls, the sputter time was decreased to 6 and 8 s and the CNT synthesis was carried out at 900 °C and 970 °C. However, this did not significantly affect the number of walls. For

instance, CNTs produced at 900 °C were mainly double-walled but with smaller diameters of about 2 nm. Decreasing the sputtering time to 7 s at 970 °C allowed us to produce mainly triple-walled and few double-walled CNTs with diameters of 3.3-7.2 nm. It was concluded that the catalyst sputter time has no effect on the variation of CNT walls.

Many catalyst particles were either completely detached or indirectly attached, i.e. not embedded inside CNTs (Figure 13). This abnormal connection between catalyst particles and CNTs can be explained by a fast quenching of the CNT growth, namely by the rapid cooling of CNTs in the dilutor when removing the sample from the reactor and sudden release of carbon which was dissolved in the catalyst particle. This could be a quite interesting approach to detach catalyst particles from CNTs and might allow synthesizing catalyst free CNTs.

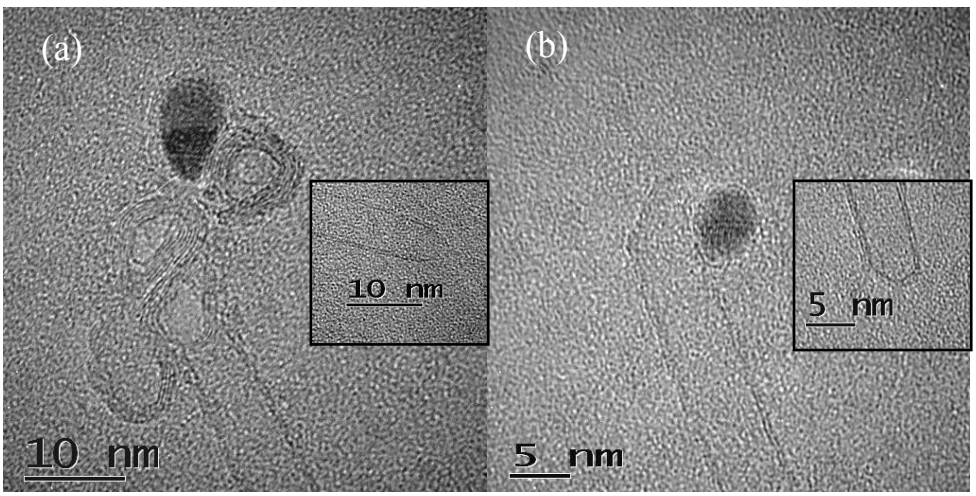

Figure 13. TEM images of CNTs together with particles that catalyzed their growth. Inset images show the other ends of the tubes. (Publication I)

FT-IR measurements of the gaseous products coming from the reactor at 900 °C were carried out during the CNT synthesis (Figure 14). When H_2 was added to Ar and CO_2

flows, the water-gas shift reaction [67] took place which led to the formation of CO and H_2O. After the introduction of CO to the reactor, 13-25 ppm of CH_4 was detected. This amount of methane, taking into account 30 min growth duration, might be sufficient for CNT growth. When CO and H_2 were switched to Ar, the CH_4 disappeared from the gaseous products.

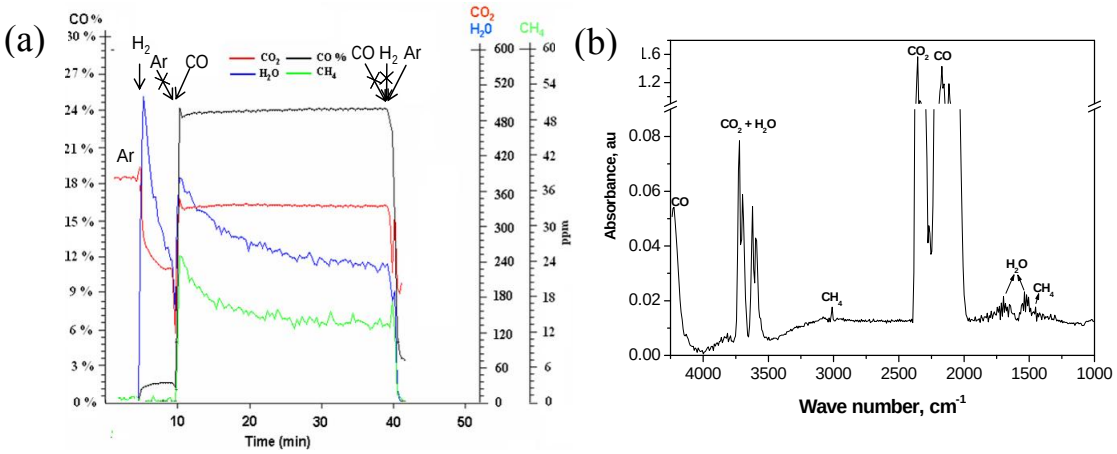

Figure 14. The results of FT-IR measurements after the reactor at 900 °C: a) time dependence of gaseous components during the process of CNT synthesis; b) IR spectrum revealing the formation of methane. (Publication I)

To examine the effect of CH_4 on the CNT structure as well as on the variation of wall numbers, additional amounts (715 and 3560 ppm) of CH_4 were added to the reactor at 900 and 970 °C. However, no significant effect on the morphology and the number of walls of CNTs was observed. Additional experiments carried out with a mixture of CH_4 and H_2, i.e. without CO, did not lead to the formation of CNTs. Therefore, methane can be ruled out as being the carbon source determining the structure and morphology of CNTs grown at high temperatures.

A thermodynamic approach was applied to examine the possible reactions in the reactor. The thermodynamic calculations were carried out using the F*A*C*T software

[68]. The values of enthalpies for different reactions were given for a temperature of 900 °C. For the calculations we used the thermodynamic data for graphitic carbon C and α-Fe.

The main source of carbon for CNT growth was the Boudouard reaction (CO disproportionation):

$$CO_{(g)} + CO_{(g)} \leftrightarrow C + CO_{2\,(g)}, \quad \Delta H = -169 \text{ kJ/mol} \qquad (5)$$

Since H_2 was also present in the reactor, another reaction, namely CO hydrogenation, leading to carbon release, could occur:

$$CO_{(g)} + H_{2\,(g)} \leftrightarrow C + H_2O_{(g)}, \quad \Delta H = -136 \text{ kJ/mol} \qquad (6)$$

Applying the rule of summation for reactions (5) and (6) one can get a water-gas shift reaction:

$$CO_{(g)} + H_2O_{(g)} \leftrightarrow H_{2\,(g)} + CO_{2\,(g)}, \quad \Delta H = -33 \text{ kJ/mol} \qquad (7)$$

determining the relative concentration of the gaseous species. Reactions (5) and (6) have very similar thermodynamic behavior [69]. At low temperatures these reactions are shifted toward the formation of carbon. A thermodynamic equilibrium ($\Delta G = 0$) is observed at a temperature of approximately 700 °C (Figure 8a). Kinetic investigations of reaction (5) show appreciable reaction rates in the temperature interval from 470 to 820 °C [69]. At higher temperatures the inverse reactions prevail. At temperatures lower than 325 °C, this reaction is limited kinetically and at high temperatures it is thermodynamically prohibited. However, reaction (5) (as well as reaction (6)) can occur

at 900 °C even though $\Delta G_{900}>0$, since the equilibrium concentration of CO_2 at this temperature is about 2.7%.

It is worth noting that the experimentally optimized concentrations of CO_2 needed for the successful CNT synthesis were close to, but smaller then the equilibrium values (Figure 15a). If the concentration of the introduced CO_2 was higher than the equilibrium one, then the equilibrium of reaction (5) would be shifted to the left and CO disproportionation would not occur. Thus, the optimized CO_2 concentration values are in good agreement with the thermodynamic approach used in this work (Figure 15a).

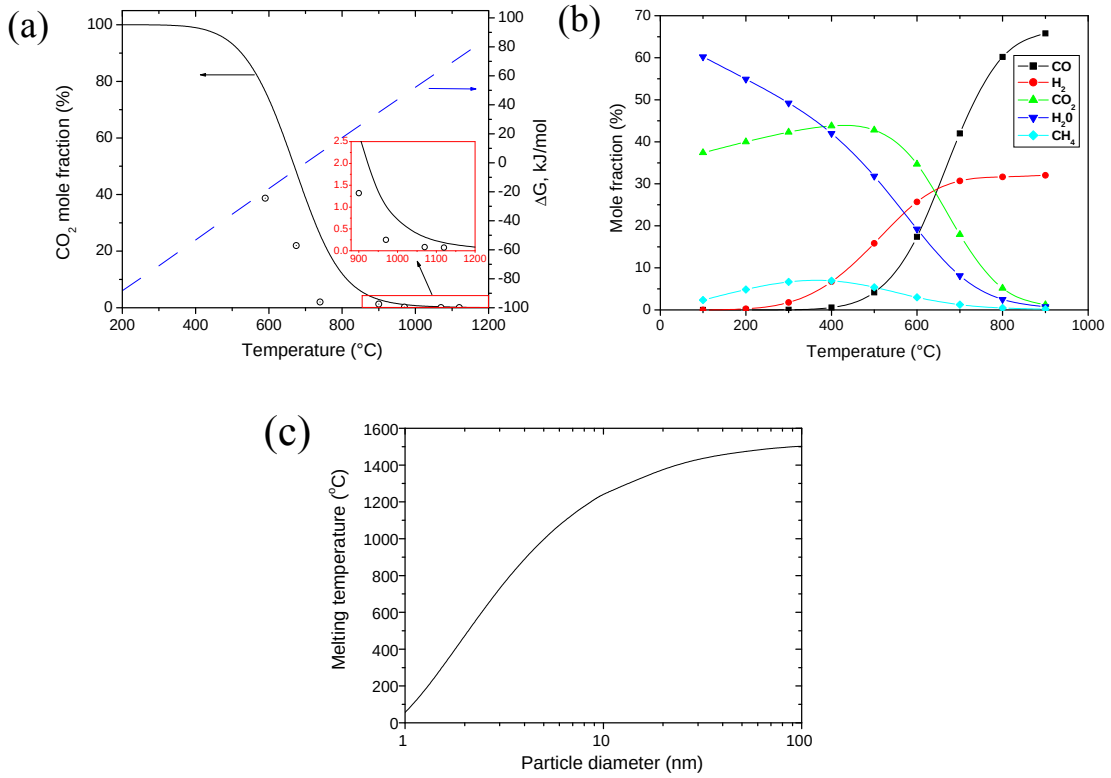

Figure 15. The results of thermodynamic calculations: a) CO disproportionation: temperature dependence of the Gibbs free energy and equilibrium CO_2 mole fraction, together with experimentally optimized concentrations for CNT growth (open dots); b) the gaseous product after mixing 2 mol CO, 1 mol H_2 and CO_2 (1.3%); c) The effect of the particle size on melting temperature of Fe particles. (Publications I, II)

As has been shown, CO_2 played a very important role in the variation of the product morphology. The absence of introduced CO_2 as well as an excess reduces the density of the CNTs, which implies disadvantageous conditions for the activation of catalyst particles. Most likely the role of CO_2 can be attributed to: i) an etching effect, i.e. removing excess and/or catalyst "poisoning" carbon or ii) the prevention of catalyst particle passivation or activation of catalyst particles according to [70]:

$$Fe_3C + CO_{2\,(g)} \leftrightarrow 3Fe + 2CO_{(g)}, \quad \Delta H = 146 \text{ kJ/mol} \tag{8}$$

since cementite is known to be an inactive phase for fiber and CNT formation [71, 72]. Reaction (8) is thermodynamically favorable ($\Delta G > 0$) at temperatures higher than 685 °C, whereas at lower temperatures the inverse reaction of cementite formation occurs. Also, one should mention the possibility of cementite formation due to the direct reaction between carbon and iron:

$$3Fe + C \leftrightarrow Fe_3C, \quad \Delta H = 12 \text{ kJ/mol} \tag{9}$$

FT-IR measurements revealed the formation of CH_4 in the reactor. This can be attributed to reactions of H_2 with CO:

$$3H_{2\,(g)} + CO_{(g)} \leftrightarrow CH_{4\,(g)} + H_2O_{(g)}, \quad \Delta H = -227 \text{ kJ/mol} \tag{10}$$

or with carbon:

$$2H_{2\,(g)} + C_{(s)} \leftrightarrow CH_{4\,(g)}, \quad \Delta H = -91 \text{ kJ/mol} \tag{11}$$

Thermodynamic calculations were performed to examine the possibility of methane formation at different temperatures in the reactor. When we calculated for a mixture of 2 mol of CO and 1 mol of H_2, corresponding to the experimental conditions (400 cm^3/min CO and 200 cm^3/min H_2), the maximum methane concentration was found to

be at around 370 °C (Figure 15b), which is in a good agreement with the literature data [73, 74]. There are two zones in the reactor with this temperature, in the upper and lower part of the reactor (Figure 7). Since methane formation requires the presence of catalyst, CH_4 was most likely formed on the reactor walls. The alumina ceramic tube used for the experiments contained SiO_2 (0.25%), Ca (0.02%), Fe (0.02%) and Cd (0.09%) impurities. The amount of the ceramic impurities was capable of producing about 10 ppm of CH_4 by this methanation process taking into account the very high surface area [75, 76]. In order to verify the methane formation on the reactor walls we replaced the ceramic tube with a quartz one. FT-IR measurements detected no methane formation coming out of the quartz tube reactor.

Incremental variation of the number of CNT walls cannot be explained by a gradual change of the reactive carbon precursor in the reactor from CO to CH_4 at high temperatures. Neither is the increase of catalyst particle size alone responsible for the formation of thin MWCNTs, since decreasing the sputtering time, i.e. decreasing the catalyst particle size, did not lead to a significant change in the number of walls of the CNTs produced, but reduced the CNT diameter.

It is known that the properties of small particles differ significantly from those of the bulk material. The melting temperature T_m for a given particle of radius r can be estimated on the basis of the Kelvin equation as

$$T_m = T_o \exp\left(-\frac{2\sigma_{sl} V}{r \Delta H_{fus}} \right), \qquad (12)$$

where T_o is the bulk melting temperature (1535 °C); ΔH_{fus} is the latent heat of fusion; V is the volume of a metal atom; σ_{sl} is the surface tension between liquid and solid. The results of the calculations are plotted in Figure 15c. As one can see, catalyst particles of 4-5 nm in diameter are expected to be in a liquid state at temperatures above 890-1000 °C.

At lower temperatures, catalyst particles are in the solid phase and, as a result, produce single-walled CNTs, which agree with the literature results [77, 78]. At high temperatures the catalyst particles are in the liquid state and promote the formation of CNTs with larger numbers of walls. These follow from the diffusion model [79-81], and can be explained by an increase in the carbon solubility [82] and diffusivity [69] in liquid iron. These properties are significantly enhanced with temperature, which also led to the increase of the length and the number of CNT walls.

The optical and electrical properties of SWCNTs strongly depend on the chiral structure of the tube [83]. For studying the properties of each particular structure, it is essential to grow individual suspended SWCNTs. Accordingly, individual SWCNTs were grown over the Si_3N_4 slit. The use of iron catalyst on the Si_3N_4 substrate did not lead to CNT growth, which is likely to be related to the reaction between iron and Si_3N_4 to form iron nitride, which is known to prevent nanotube growth. Nickel employed as a catalyst initiated CNT growth in a CO atmosphere. SWCNTs were synthesized at 740 °C by keeping the slits in the direction of gas flow. Figure 16 shows a typical SWCNT grown across the slit.

By using a method based on intrinsic layer line distance analysis [84], the diffraction pattern (Figure 16b) was indexed and the chiral indices were determined to be (28, 14) with a diameter of 2.9 nm, which is in a good agreement with the Raman spectra (Figure 16c). Using a relation between the frequency of the radial breathing mode (RBM) mode (ω_{RBM}) and the diameter of the tube, $d = 227.0/\omega_{RBM}$, obtained for a large number of long isolated SWCNTs grown by a "supergrowth" method, we get another estimate for the diameters of the tubes [85]. The frequency of the RBM mode for the tube is 75.8 cm^{-1} giving a diameter of 3.0 nm. On the other hand, using the relationship $d = 204/(\omega_{RBM}-27)$, which was obtained for suspended SWCNTs leads to a severe overestimate of the diameters (3.2 nm) [86]. This discrepancy shows that still more work is needed to fully understand the different factors that affect the relationship between the diameter and the frequency of the RBM. This method is an efficient way to grow individual CNTs for the investigations of transport, optical and sensing properties of individual SWCNTs. In particular, the nonlinear optical response of well characterized individual semiconducting SWCNTs was studied from these grown SWCNTs [Publication III].

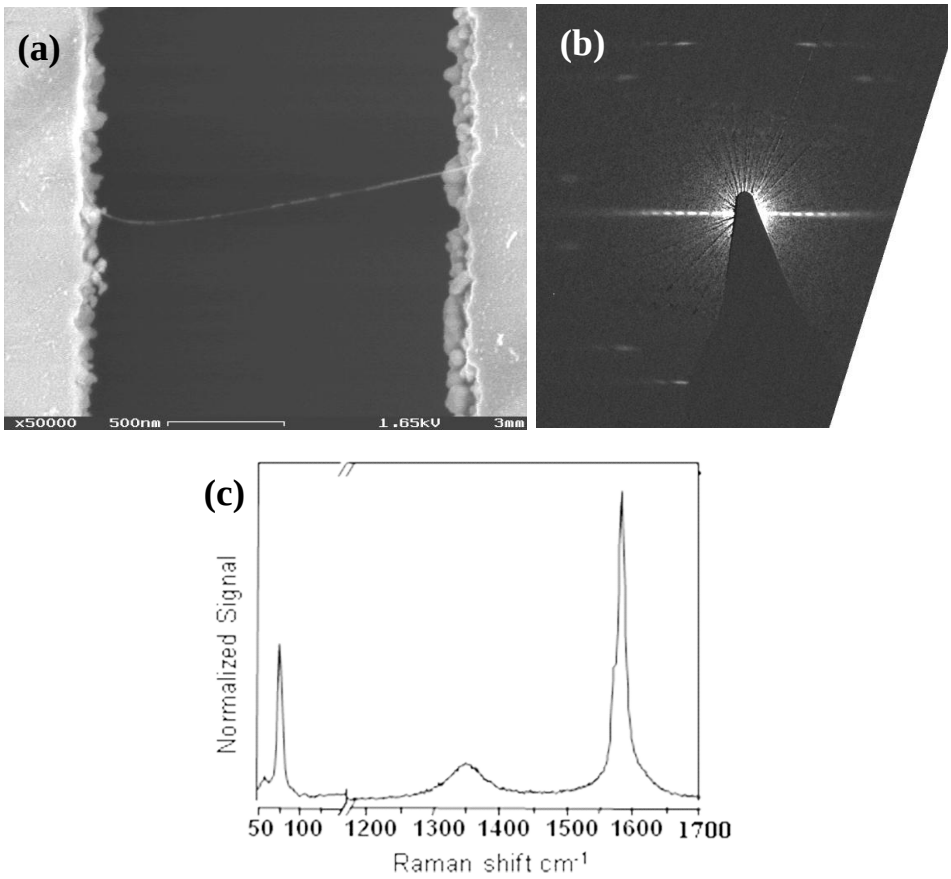

Figure 16. Individual SWCNT grown across a Si_3N_4 slit: a) SEM image; b) and c) electron diffraction pattern and Raman spectra of the particular SWCNT. (Publication III)

4.2 CNT/CNF synthesis on particles

4.2.1 Synthesis in horizontal CVD reactor

Both silica and cement particles were completely covered by carbon nanomaterials when acetylene was used as the carbon source. On the surface of silica particles, mostly CNFs with diameters varying from 30 to 50 nm, were observed at a growth temperature of 550 °C. Increasing the temperature resulted in the growth of MWCNTs [87] with 5 to 10 walls, as shown in Figure 17. The outer diameter of the MWCNTs varied from 10 to

15 nm at 600 °C and from 12 nm to 20 nm at 750 °C. The maximum length of the CNTs was found to be 15 μm.

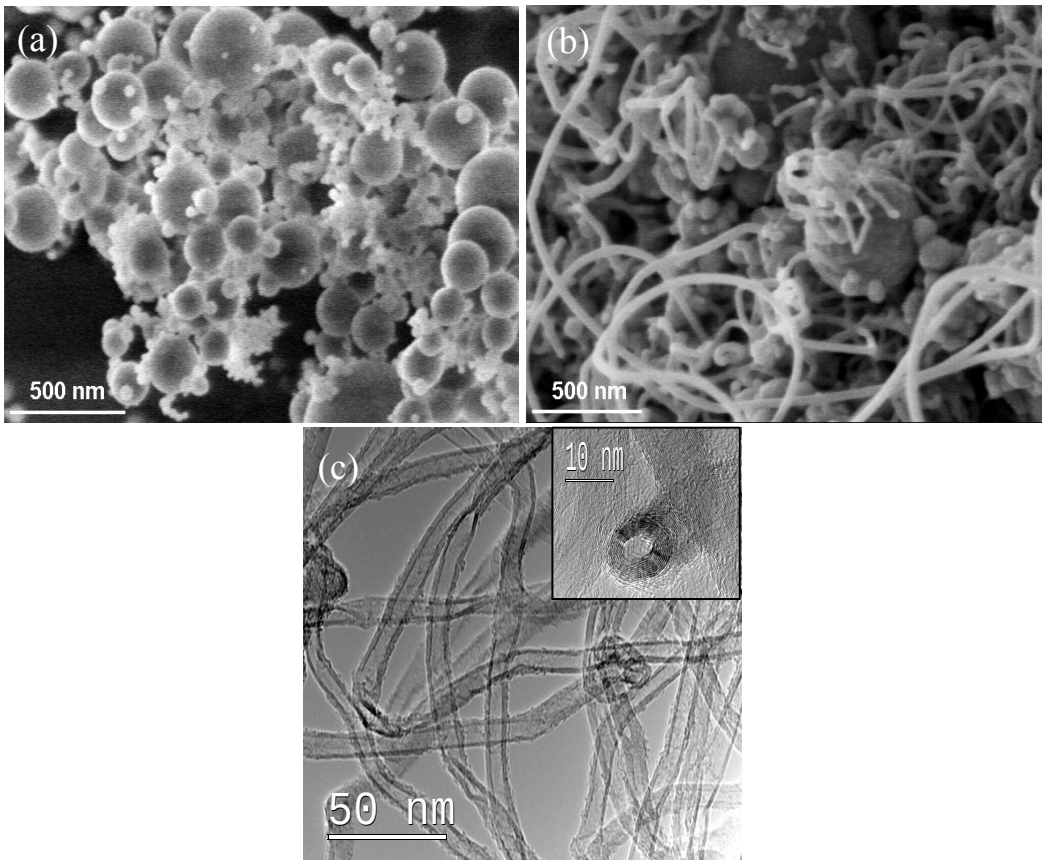

Figure 17. SEM images: **a)** pristine silica particles; **b)** silica particles treated at 600 °C at the synthesis conditions; **c)** TEM image of CNTs grown at 600 °C on the surface of silica particles. (Publication IV)

On the surface of cement particles we synthesized a novel cement hybrid material (CHM), in which CNFs are attached to the cement particles. Cement is known to consist of the oxide components (SiO_2, MgO and Al_2O_3), which are good supporting materials for the growth of CNTs and CNFs [e.g., 9, 10, 14]. CNFs with diameters of about 30 nm and average lengths 3 μm were grown under the same conditions used for the growth on cement particles (Figure 18), giving a maximum yield of 20%. The difference between the products synthesized on silica and cement particles gave us grounds for the suggestion that the amount of catalyst was not sufficient in the cement particles. In

order to examine this hypothesis, cement particles were impregnated with iron salt. For the impregnation, however, utilization of the impregnated cement particles slightly increased the yield of CNFs, but did not lead to the formation of CNTs.

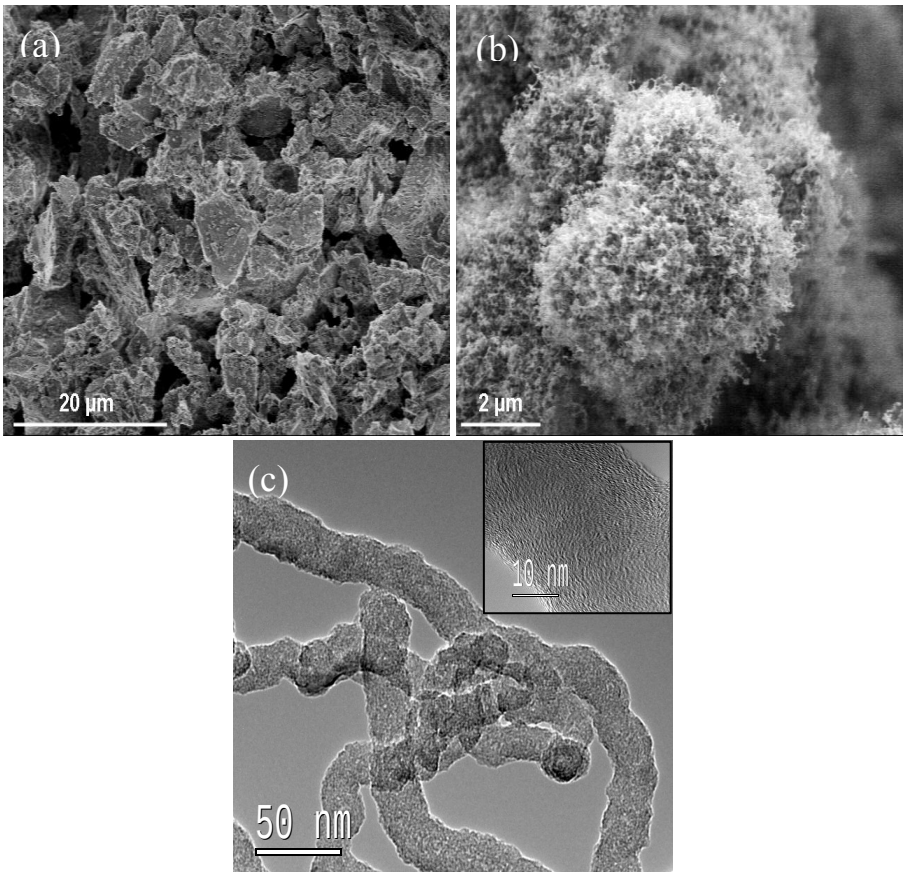

Figure 18. SEM images of **(a)** pristine cement particles and **(b)** cement treated at 650 °C at the synthesis conditions; **(c)** TEM image of CNTs and CNFs grown at 650 °C on the surface of cement particles. (Publication IV)

In order to examine the possible changes of cement at high temperatures, X-ray powder diffraction (XRD) analysis was used. No major changes were found in the cement particles up to 700 °C, but new peaks corresponding to graphitized carbon appeared in the diffraction pattern (Figure 19). Also, the gypsum phase vanished after the treatment at high temperatures, which was explained by a gradual 2 stage dehydration process of gypsum ($CaSO_4 \cdot 2H_2O$) in the temperature ranges of 120-180 ^oC and 180-230 ^oC, with

the final formation of the crystalline anhydrite ($CaSO_4$) phase at about 450 °C [88]. The intensities of the other peaks of different crystalline cement compounds such as Ca_3SiO_5, Ca_2SiO_4 and $Ca_3Al_2O_6$ essentially did not change under the synthesis conditions. Heat treatment of cement particles at 900 °C led to the formation of free lime phase, CaO, probably due to the decomposition of the alite phase (Ca_3SiO_5) to Ca_2SiO_4 [89]. The alite phase is the main component for providing strength in cement [90]. Due to decomposition of the alite phase the strength of the cement decreased. Thus, from the XRD data it can be concluded that the conditions of CNF and CNT synthesis did not significantly change the composition of the cement particles. Therefore, the produced carbon nanomaterials would be easily and homogenously dispersed in the concrete and mortar and could be intermingled with the products during the cement hydration process.

Gypsum is usually added and mixed with clinker at the final stage of cement production and used mainly as an inhibitor for cement hydration process. For industrial applications, clinker particles should be used instead of cement. This will first make the process of CNT/CNF-cement composite manufacturing cheaper and secondly will allow the avoidance of chemical changes in the cement material. In order to confirm the possibility of using clinker as a catalyst and a support, similar investigations were carried out with acetylene. No significant difference in the products was observed between cement and clinker.

The procedure described above for the synthesis of carbon nanomaterials did not produce CNTs and CNFs on cement particles using CH_4 as a carbon source. This can be explained by the need of high temperatures (850-950 °C) for CH_4 decomposition. At

these temperatures cement particles change their crystal structure, as was found by XRD investigations (Figure 19). On-line Fourier-Transform Infrared (FT-IR) measurements of the outlet gas phase composition revealed relatively high emissions of CO_2 and H_2O in Ar atmosphere during heating of the cement particles [91]. These two gaseous compounds are known to behave as etching agents [92] and could completely suppress the growth of CNTs and CNFs on the surface of cement particles.

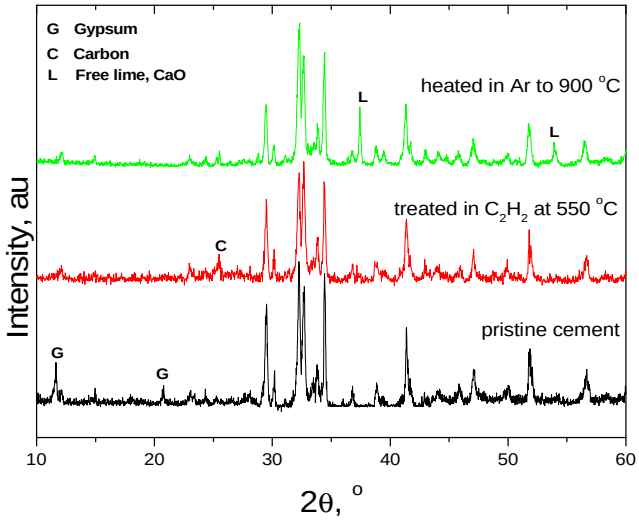

Figure 19. XRD patterns of pristine cement particles, the product after the synthesis at 550 ºC on the cement surface and cement after the heat treatment at 900 ºC in Ar atmosphere. (Publication IV)

4.2.2 Synthesis in screw feeder reactor

In the screw feeder reactor the product deposited on the cement particles varied from no carbon (below 450 °C) to complete coverage at higher temperatures. TEM images confirmed the formation of CHM, showing that CNTs and CNFs were attached to cement particles (Figure 20). These structures provided a good dispersion of the CNTs and CNFs in the cement matrix, which is essential for creation of very strong and electrically conductive concrete materials.

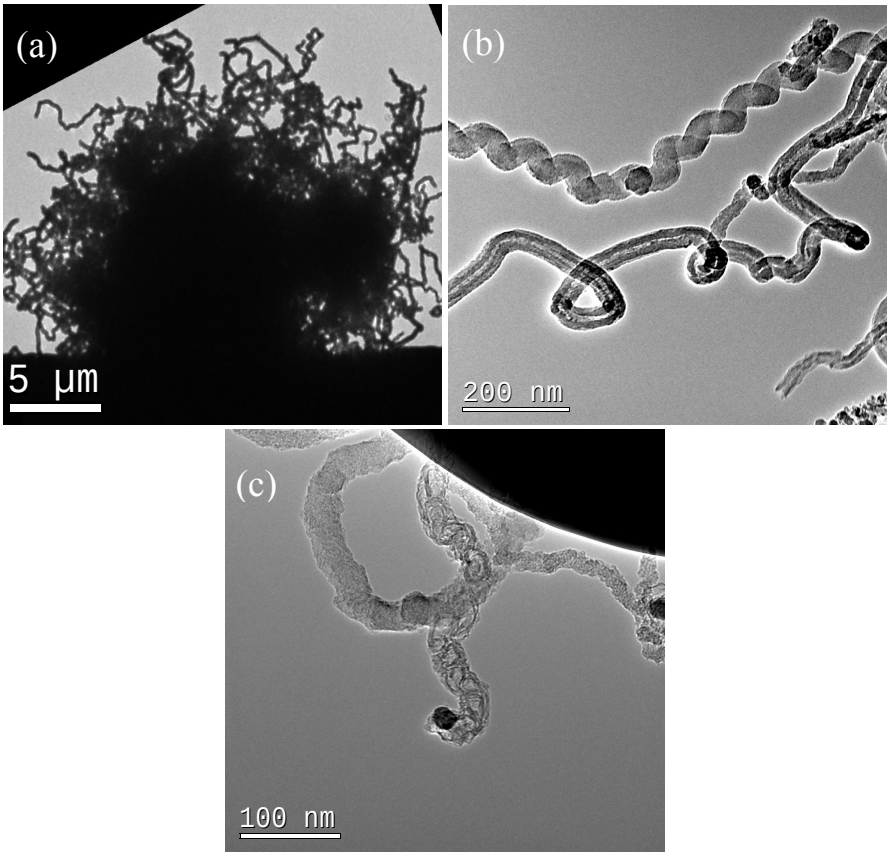

Figure 20. TEM images of CHM structures **a)** showing complete coverage of the cement particles by carbon material. **b)** and **c)** revealing the formation of multiwalled CNTs and CNFs. (Publication V)

The CNT/CNF yield was estimated on the basis of the change of the cement color from light-brown to black. For quantitative determination of the carbon nanomaterial yield, thermogravimetric analysis (TGA) was performed in air using a Netzsch STA 449C thermobalance. The results showed two features in the temperature ranges 80-280 and 380-560 °C for the SR CHM (Figure 21a). The low temperature mass decrease can be attributed to hydrocarbons, which were formed due to acetylene polymerization reactions [93]. The second step can be explained by burning out of carbon from the CNTs and CNFs. Table 5 shows the effect of the experimental conditions on the product yields calculated based on the TG analysis results per mass of raw cement (Y_{cem}) or iron (Y_{Fe}) contained in the cement.

Table 5. Effect of experimental conditions of the carbon material yield obtained on the basis of TGA data and calculated per mass of cement (Y_{cem}) or iron (Y_{Fe}).

T [^{o}C]	C_2H_2 [cm^3min^{-1}]	CO_2 [cm^3min^{-1}]	CO [cm^3min^{-1}]	Y_{cem} [%]	Y_{Fe} [%]
525	660	660	0	6.6	240
525	660	660	50	4.9	180
525	0	0	50	0	0
525	660	0	50	33	1150
550	860	0	50	46	1660
550	860	0	177	37	1330
600	860	0	50	45	1610
550[a]	860	0	50	3.3	1430

[a] White cement

The most reactive system, resulting in the highest carbon yield of Y_{Fe} = 1660% corresponding to 15 g/hour, was found to be a mixture of acetylene and CO. Interestingly, addition of equimolar concentrations of CO_2 to acetylene did not lead to the increase of CNT yield that would have been expected from the literature [94, 95]. CO alone, known to be a good carbon precursor for single-walled CNT production [96-98], did not form any carbon product at these low temperatures. Nevertheless, the important role of CO can be attributed to the reduction of iron oxide [99]. Even though the absolute yield of carbon nanomaterials was significantly higher for SR cement, the yield calculated per mass of available iron was found to be very similar for SR and White cements.

Raman spectra were recorded using a frequency-doubled Nd:YAG green laser (532.25 nm, 30 mW) and CCD detector in ambient conditions. Results for the as-grown hybrid CNT modified cement samples showed two main features in the spectra, the G band at

about 1600 cm^{-1} and D band at 1325 cm^{-1} (Publication V), which respectively indicate the presence of graphitized (sp^2-hybridized) and amorphous or sp^3-hybridized carbon in the samples. These are typical spectra obtained for MWCNTs [100]. The results of the Raman measurements did not significantly change when the type of cement or experimental conditions were varied. XRD analysis revealed that no major changes were found in the crystallinity, but new peaks corresponding to graphitized carbon appeared and the gypsum phase vanished (Figure 21b) in the same way as discussed in the previous section.

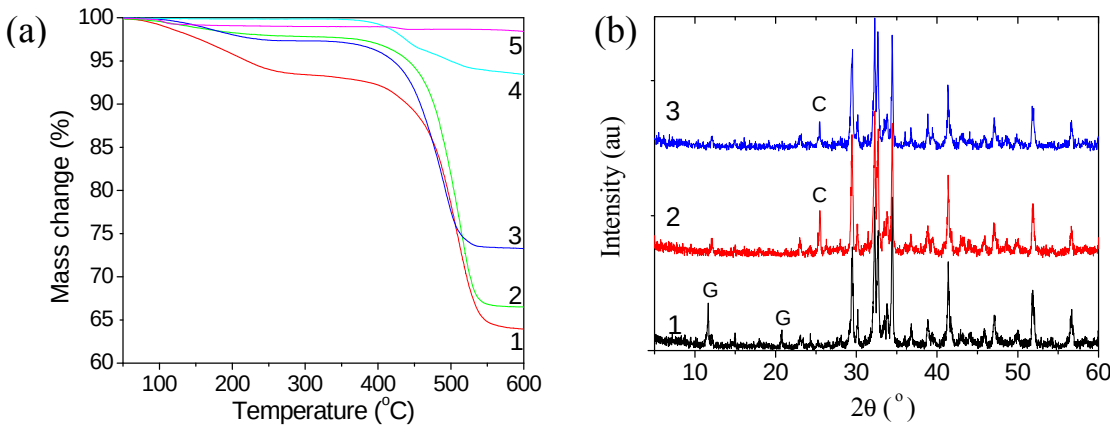

Figure 21. a) TGA curves of CHM produced (1) at 600 °C and (2) at 550 °C under C_2H_2 + CO (860 + 50 cm^3min^{-1}), (3) at 525 °C under C_2H_2 + CO (660 + 50 cm^3min^{-1}), and (4) at 525 °C under C_2H_2 + CO_2 (660 + 660 cm^3min^{-1}), and (5) pristine SR cement; b**)** XRD patterns of (1) pristine SR cement and CHM produced (2) at 500 ºC in C_2H_2 + CO_2 (500 + 500 cm^3min^{-1}), (3) at 575 ºC under C_2H_2 + CO_2 (660 + 60 cm^3min^{-1}) reveal the gypsum (G) decomposition under thermal treatment and appearance of the graphitized carbon (C). (Publication V)

4.2.3 Application for construction materials

To examine the quality of the produced hybrid structures for applications in construction material, hardened cement paste (concrete without sand and gravel) was prepared from the produced CHM. Compressive and flexural strength as well as

electrical conductivity measurements were carried out. For the current tests, beams with dimensions of 60x10x10 mm^3 were prepared using Teflon molds and cured in water at 20 ºC for 7, 14 and 28 days. Each series consisted of three beams. The cement paste specimens produced from a mixture of pristine SR cement and SR CHM contained a polycarboxylate based surfactant available under the commercial name Kollomент (Grace Chemicals), whereas the cement paste specimens produced entirely from SR CHM contained a mixture of two surfactants, Kollomент and Parmix (Finnsementti Oy). The cement paste beams were first tested to determine their flexural strength. Then, three out of six half-beams were crushed to determine compressive strength while the remaining half-beams were used for the electrical resistance measurements. The electrical resistance, R, of the concrete samples dried at ambient conditions after one day and two months after the mechanical investigations, was measured using two contacts pressed on to opposite sides of the sample through soft graphite films with an area of S = 1 cm^2 separated by a distance L =1.2 cm. The resistivity, ρ was determined as $\rho = R \cdot S / L$.

The strength tests after 7 and 14 days after curing in water showed a slight worsening of the mechanical properties of samples when the ordinary cement was partially or completely replaced by CHM. This might be explained by a lower degree of hydration of the modified cement. After two months drying at ambient conditions the most significant decrease in the concrete electrical conductivity was observed for the samples made using the highest amount of pristine cement, while no time effect was found for the samples when 100% CHM samples had been used.

The cement pastes made of CHM samples produced using different conditions confirmed the significant improvement of both mechanical and electrical properties after curing in water for 28 days. This improvement was due to the good interfacial bonding between CNFs and cement. As seen from Table 6, the SR CHM can be used to prepare a mechanically very strong paste with compressive strength more than 2 times higher than that of the paste prepared from the pristine cement. In addition, up to 40 times better electrical conductivity can be produced in our paste whilst preserving its mechanical properties.

To the best of our knowledge, these significant compressive strength and electrical conductivity enhancements are the highest reported with the help of CNTs. Up to now, CNTs and CNFs added to cement matrix have resulted in either a decrease or a rather small (up to 20%) increase of the compressive strength [101-103]. The main problem has been to obtain a good dispersion of carbon nanomaterials in the matrix. On the other hand, the weakest point for the composites, using carbon nanostructures for advanced materials, is in the interfacial bonding between CNTs and the binder matrix. In order to improve this situation, many researchers [101, 104-108] have treated CNTs/CNFs with, for example, ozone gas or silane or sulfuric or nitric acids leading to the formation of carboxylic groups capable of enhancing the reinforcement efficiency between the hydrated cement and the CNTs. From this point of view, in order to increase the strength of the hardened paste (or concrete) it is essential to attach or produce CNTs/CNFs attached to cement particles, as we have demonstrated in this work. In this way, the carbon nanomaterials are easily and homogenously dispersed in the cement paste and are intermingled with the hydration products during the hydration process.

It is important to note that the best mechanical results were obtained from the CHM synthesized in the presence of CO_2, while the component needed for the highly conductive paste was fabricated by adding CO to the reactor. If the increase in the electrical conductivity can be explained by higher CNT and CNF yield in the presence of carbon monoxide, the role of CO_2 might be attributed to the etching of amorphous carbon and hydrocarbons formed due to C_2H_2 polymerization.

Table 6. Mechanical (after 28 days curing in water) and electrical (1 day after mechanical testing) properties of cement paste prepared by adding different samples of SR CHM.

Fraction of CHM [%]	Synthesis conditions				Compressive strength [MPa]	Electrical resistivity [MΩ·cm]
	Temperature [ºC]	Gas flow rate, [cm^3min^{-1}]				
		C_2H_2	CO_2	CO		
0	-	-	-	-	25	9.7
100	550[a]	860	0	177	22	0.23
100	575[b]	660	660	0	55	1.3
100	500[b]	500	500	0	40	1.7
100	525	660	660	0	56	4.0

[a] 6 min^{-1} and [b] 2 min^{-1} – screw feeder rotation rate.

SEM observations together with EDX analyses found that the CNTs and CNFs originally attached to the cement particles appeared to be embedded in the hydration products (Figure 22). CNTs and CNFs bridged the neighboring cement particles surrounded by their hydration products, which led to the significant increases in the mechanical strength and electrical conductivity on the hardened paste.

Significant enhancement of the mechanical properties of the SR CHM paste after prolonged water curing was certainly caused by progressing hydration. The results also

indicate a significantly slower hydration rate of the CHM in comparison with the pristine cement. The difference between the strengths of CHM and pristine cements can be partly explained by the change of gypsum to its anhydrite form. $CaSO_4$ has a slower dissolution rate compared to gypsum and thereby could be lacking in the pore water to hinder the reaction of the $Ca_3Al_2O_6$ clinker phase in the early stages of cement hydration. Also, $CaSO_4$ in cement reacts with batch water and transforms into hemi hydrate/gypsum so the volume of water available for hydration of calcium silicate hydrate, which is responsible for the good strength properties of concrete, is decreased [88]. This could also contribute in the stiffening of the paste in CHM hydration.

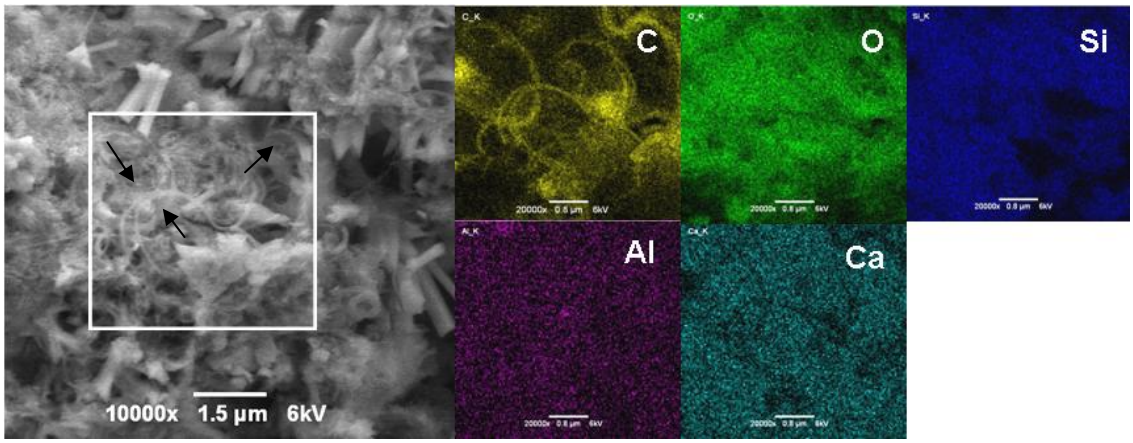

Figure 22. The results of SEM/EDX investigations of the hardened cement paste (curing in water for 28 days) after the mechanical test. The images reveal the presence of carbon nanomaterials (indicted by arrows) and cement composition elements: O, Al, Si and Ca. (Publication V)

5 Conclusions

This thesis reports the synthesis of carbon nanomaterials on flat substrates and on micron sized particles in three different CVD reactors. In the vertical CVD reactor, CNTs were grown on flat silica substrates using CO and Fe as a carbon source and a catalyst, respectively. It was shown that the CNT morphology can be controlled by the catalyst sputtering time and by the amount of CO_2 introduced in the reactor. It was found that CO_2 plays a crucial role in the CNT growth, which was attributed to etching of amorphous carbon and prevention of the formation of the cementite phase. Depending on the synthesis conditions, the diameter of the CNTs can be varied from 1.4 to 12 nm. A variation of the number of CNT walls from 1 to 4 was found by changing the synthesis temperature from 590 to 1070 °C, together with CO_2 concentration. Increasing the temperature resulted in an increase in the CNT length from 0.5 to 350 μm. This incremental variation of the number of CNT walls and CNT length with growth temperature can be explained by an enhancement of carbon solubility and diffusivity. To study individual SWCNT properties, we developed a method for nanotube growth across a 1.5 μm width Si_3N_4 slit. Both TEM and Raman characterization techniques were employed to study the properties of the grown SWCNTs.

By using the horizontal CVD reactor, we showed, for the first time, the possibility to synthesize CNFs on cement and clinker without additional catalyst. The carbon nanomaterials produced in this way are homogenously dispersed in the matrix materials, which solves the major problem of creating a good dispersion of CNTs and CNFs in a

matrix and also provides good bonding between carbon and matrix materials. XRD characterization revealed no major change in the cement crystallinity up to the synthesis temperature of 700 °C, but a new peak corresponding to graphitized carbon appeared, and the gypsum phase vanished. Utilization of silica fume particles impregnated by iron salt provided a model material for a comparison with cement particles. Increasing the synthesis temperature from 550 to 750 °C resulted to the change of the product from CNFs to CNTs.

Since the horizontal CVD reactor allowed us to synthesize a maximum of about 150 mg h^{-1} of the nanomaterials on the surface of cement, we elaborated and constructed a continuous CVD reactor based on screw feeding of the catalyst. The optimization of the experimental conditions (the rate of the catalyst feeding, the flow rate and the concentration of acetylene and promoting gases such as CO and CO_2) allowed us to increase the yield up to 30 g h^{-1}. This amount was sufficient for the mechanical tests of the composite material. Investigations of the physical properties of the paste made of the CHM revealed as high as a 2-fold increase in the compressive strength and a 40-fold increase in the electrical conductivity after 28 days curing in water, which are the highest so far reported.

6 References

1. Radushkevich, L.V., Lukyanovich, V.M. Sov. J. Phys. Chem. 1952; 26: 88-95.

2. Hillert. M., Lange N. Zeitschr. Kristallogr 1958; 111: 24-34.

3. Bollmann, W., Spreadborough, J. Nature 1960; 186: 29-30.

4. Oberlin, A., Endo, M., Koyama, T. J. Cryst. Growth 1976; 32: 335-49.

5. Kroto, H.W., Heath J.R., O'Brien, S.C., Curl, R.F., Smalley, R.E. Nature 1985; 318: 162-3.

6. Iijima, S. Nature 1991; 354: 56-58.

7. Ijima, S., Ichihashi, T. Nature 1993; 363: 603-5.

8. Bethune, D.S., Kiang, C.H., De Vries, M.S., Gorman, G., Savoy, R., Vazquez, J., Beyers, R. Nature 1993; 363: 605-7.

9. Carneiro, O.C. Anderson, P.E., Rodriguez, N.M., Baker, R.T.K. J. Phys. Chem. B, 2004; 108: 13307-14.

10. Colomer, J.-F., Stephan, C., Lefrant, S., Van Tendeloo G., Willems, I., Konya, Z., Fonseca, A., Laurent, Ch., Nagy, J.B. Chem. Phys. Lett. 2000; 317: 83-9.

11. Lyu, S.C., Liu, B.C., Lee, T.J., Liu, Z.Y., Yang, C.W., Park, C.Y., Lee, C.J. Chem. Commun. 2003; 734-5.

12. Chopra, N., Hinds, B. Inorg. Chim. Acta 2004; 357: 3920-26.

13. Pinheiro, J.P., Schouler, M.C., Gadelle, P. Carbon 2003; 41: 2949-59.

14. Thaib, A., Martin, G.A., Pinheiro, P., Schouler, M.C., Gadelle, P. Catal. Lett. 1999; 63: 135-41.

15. Mukhopadhyay, K., Koshio, Sugai, T., Tanaka, N., Shinohara, H., Konya, Z., Nagy, J.B. Chem. Phys. Lett. 1999; 303: 117-24.

16. Couteau, E., Hernadi, K., Seo, J.W., Thien-Nga, L., Miko, Cs., Gaal, R., Forro, L. Chem. Phys. Lett. 2003; 378: 9-17.

17. Kong, J., Soh, H.T., Cassell, A.M., Quate, C.F., Dai, H. Nature 1998; 395: 878-81.

18. Huang, S., Cai, X., Liu, J. J. Am. Chem. Soc. 2003; 125: 5636-37.

19. Zheng, B., Lu, C., Gu, G., Makarovski, A., Finkelstein, G., Jie Liu, J. Nano Lett. 2002; 2: 895-8.

20. Peng H.B.; Ristroph, T.G., Schurmann G.M., King, G.M., Yoon, J., Narayanamurti, V., Golovchenko, J.A. Appl. Phys. Lett. 2003; 83: 4238-40.

21. Kasumov, Y.A., Shailos, A., Khodos, I.I., Volkov, V.T., Levashov, V.I., Matveev, V.N., Guéron, S., Kobylko, M., Kociak, M., Bouchiat, H., Agache, V., Rollier, A.S., Buchaillot, L., Bonnot, A.M., Kasumov, A.Y. Appl. Phys. A. 2007; 88: 687-91.

22. Ward, J.W., Wei, B.Q., Ajayan, P.M. Chem. Phys. Lett. 2003; 376: 717-25.

23. Bai, J.B. Mater. Lett. 2003; 57: 2629-33.

24. Murakami, Y., Chiashi, S., Miyauchi, Y., Hu, M., Ogura, M., Okubo, T., Maruyama, S. Chem. Phys. Lett. 2004; 385: 298-303.

25. Han, S., Liu, X., Zhou, C. J. Am. Chem. Soc. 2005; 127: 5294-5.

26. Varanasi, C., Petry, J., Brunke1, L., Yang, B.T., Lanter, W., Burke, J., Wang, H., Bulmer, J.S., Scofield, J., Barnes, P.N. Carbon 2010; 48: 2442-6.

27. Chen, J., Gao, F., Zhang, L., Huang, S. Mater. Lett. 2009; 63: 721-3.

28. Dresselhaus, M.S., Dresselhaus, G., Avouris, Ph. Carbon Nanotubes: synthesis, structure, properties, and applications. Springer-Verlag, Berlin Heidelberg, 2001.

29. Dresselhaus, M.S., Dresselhaus, G., Saito, R. Carbon, 1995; 33: 883-91.

30. Teo, K.B.K., Singh, C. Chhowalla, M. Milne, W.I. Encyclopedia of Nanoscience and Nanotechnology, vol. 1, Ed. Nalwa, H.S., American Scientific Publishers, Stevenson Ranch, CA, USA, 2004; 666 p.

31. Rodriguez, N.M., Chambers A., Baker, R.T.K. Langmuir 1995; 11: 3862-6.

32. Downs, W.B., Baker, R.T.K., J. Mater. Res. 1995; 10: 625-33.

33. Koo, J.H. Polymer Nanocomposites: processing, characterization, and applications. McGraw-Hill Nanoscience and Technology Series, 2006; 22 p.

34. Baughman, R.H., Zakhidov, A.A., de Heer, W.A. Science 2002; 297: 787-92.

35. Kong, J., Franklin, N.R., Zhou, C., Chapline, M.G., Peng, S., Cho, K., Dai, H. Science 2000; 287: 622-626.

36. Niu, C., Sichel, E.K., Hoch, R., Moy, D., Tennent, H. Appl. Phys. Lett. 1997; 70: 1480-82.

37. Novak, J.P., Lay, M.D, Perkins, F.K. Snow, E.S. Solid State Electron. 2004; 48: 1753-6.

38. Lee, N.S., Chung, D.S., Han, I.T., Kang, J.H., Choi, Y.S., Kim, H.Y., Park, S.H., Jin, Y.W., Yi, W.K., Yun, M.J., Jung, J.E., Lee, C.J., You, J.H., Jo, S.H., Lee, C.G., Kim, J.M. Diam. Relat. Mater. 2001; 10: 265-70.

39. Srivastava, A., Srivastava O.N., Talapatra, S., Vajtai R., Ajayan, P.M. Nat. Mat. 2004; 3: 610-4.

40. Chu, B.T.T., Tobias, G., Salzmann C.G., Ballesteros B., Grobert N., Todd R.I., Green, M.L.H. J. Mater. Chem. 2008; 18: 5344-49.

41. Li, G.Y., Wang, P.M., Zhao, X. Carbon 2005; 43: 1239-45.

42. Bessel, C.A., Laubernds, K., Rodriguez, N.M., Terry, R., Baker, K. J. Phys. Chem. B 2001; 105: 1115-8.

43. Adhyapak, P.V., Maddanimath, T., Pethkar, S., Chandwadkar, A.J., Negi, Y.S., Vijayamohanan, K. J. Power Sources 2002; 109: 105-10.

44. Vamvakaki, V. Tsagaraki, K., Chaniotakis, N. Anal. Chem. 2006; 78: 5538-42.

45. Jang, J., Bae, J. Sens. Actuator B-Chem 2007; 122: 7-13.

46. Ma, Z., Kotaki, M., Inai, R., Ramakrishna, S. Tissue Eng. 2005; 11: 101-9.

47. Hammel, E., Tang, X., Trampert, M., Schmitt, T., Mauthner, K., Eder, A., Pötschke, P. Carbon 2004; 42: 1153-8.

48. Ebbesen, T.W., Hiura, H., Fujita, J., Ochiai, Y., Matsui, S., Tanigaki, K. Chem. Phys. Lett. 1993; 209: 83-90.

49. Waldorff, E.I., Waas, A.M., Friedmann, P.P., Keidar, M., J. Appl. Phys. 2004; 95: 2749-54.

50. Guldi D.M., Martin, N. Carbon Nanotubes and Related Structures Synthesis, Characterization, Functionalization, and Applications. Wiley-VCH, Weinheim, 2010; 4-5 pp.

51. Yakobson, B.I., Smalley, R.E. Am. Sci. 1997; 85: 324-37.

52. Dupuis, A.-C. Prog. Mater. Sci. 2005; 50: 929-61.

53. Steiner, S.A., Baumann, T.F., Bayer, B.C., Blume, R., Worsley, M.A., MoberlyChan, W.J., Shaw, E.L., Schlogl, R., Hart, A.J., Hofmann, S., Wardle, B.L. J. Am. Chem. Soc. 2009; 131: 12144-54.

54. Uchino, T., Bourdakos, K.N., de Groot, C.H., Ashburn, P., Kiziroglou, M.E., Dilliway, G.D., Smith, D.C. Appl. Phys. Lett. 2005; 86: 233110-1-3.

55. Liu B., Ren, W., Gao, L., Li, S. Pei, S., Liu, C., Jiang, C., Cheng, H. J. Am. Chem. Soc. 2009; 131: 2082-3.

56. Unalan, H.E., Chhowalla, M. Nanotechnology 2005; 16: 2153-63.

57. Vajtai, R., Kordas, K., Wei, B.Q., Bekesi, J., Leppävuori, S., Ajayan, P.M. Mater. Sci. Eng. C 2002; 19: 271-4.

58. Hata, K., Futaba, D.N., Mizuno, K., Namai, T., Yumura, M., Iijima, S. Science 2004; 306: 1362-4.

59. Masuda, T., Mukai, S.R., Hashimoto, K. Carbon 1993; 31: 783-7.

60. Fan, Y.-Y., Li, F., Cheng, H.-M., Su, G., Yu, Y.-D., Shen Z.-H. J. Mater. Res.1998; 13: 2342-6.

61. Kamalakaran, R., Terrones, M., Seeger, T., Koholer-Redlich, Ph., Ruhle, M., Kim, M.A., Hayashi, T., Endo, M. Appl. Phys. Lett. 2000; 77: 3385-8.

62. Andrews, R., Jacques, D., Rao, A.M., Derbyshire,F., Qian D., Fan, X. Chem Phys Lett. 1999; 303: 467-74.

63. Cheng, H.M., Li, F., Su, G., Pan, H.Y., He, L.L., Sun, X., Dresselhaus, M.S. Appl. Phys. Lett. 1998; 72: 328-4.

64. Nasibulin, A.G., Moisala, A., Brown, D.P., Jiang, H., Kauppinen, E.I. Chem. Phys. Lett. 2005; 402: 227-32.

65. Ahonen, P.P., Moisala, A., Tapper, U., Jokiniemi, J.K., Kauppinen, E.I. J. Nanopart. Res. 2002; 4: 43-52.

66. Weng, J.K., Langan, B.W., Ward, M.A. Can. J. Civ. Eng. 1997; 24: 754-60.

67. Nasibulin, A.G., Brown, D.P., Queipo, P., Gonzalez, D., Jiang, H., Kauppinen, E.I. Chem. Phys. Lett. 2006; 417: 179-84.

68. Bale, C.W., Chartrand, P., Degterov, S.A., Eriksson, G., Hack, K., Mahfoud R.B., Melancon, J., Pelton, A.D., Petersen, S. Calphad-Comput. Coupling Ph. Diagrams Thermochem. 2002; 26: 189-228.

69. Nasibulin, A.G., Queipo, P., Shandakov, S.D., Brown, D.P., Jiang, H., Pikhitsa, P. V., Tolochko, O.V., Kauppinen, E.I. J. Nanosci. Nanotechnol. 2006; 6: 1233-46.

70. Audier, M., Coulon, M., Bonnetain, L. Carbon 1983; 21: 93-7.

71. Baker, R.T.K., Alonzo, J.R., Dumesic, J.A., Yates, D.J.C. J. Catal. 1982; 77: 74-84.

72. Hernadi, K., Fonseca, A., Nagy, J.B., Fudala, A., Bernaerts, D., Kiricsi, I. Appl. Catal. A 2002; 228: 103-13.

73. Lo, J.M.H., Ziegler, T. J. Phys. Chem. C 2007; 111: 11012-25.

74. Sehested, J., Larsen, K.E., Kustov, A.L., Frey, A.M., Johannessen, T., Bligaard, T., Andersson, M.P., Norskov, J.K., Christensen, C.H. Top. Catal. 2007; 45: 9-13.

75. Tahir, A.H.K. Methanation-Bimetallic Catalysts. Ph.D. Thesis, University of the Punjab, Pakistan, 1992.

76. Choudhury, M.B.I., Ahmed, S., Shalabi, M.A., Inui, T. Appl. Catal. A-Gen. 2006; 314: 47-53.

77. Maruyama, S., Kojima, R., Miyauchi, Y., Chiashi, S., Kohno, M. Chem. Phys. Lett. 2002; 360: 229-34.

78. Bachilo, S.M., Balzano, L., Herrera, J.E., Pompeo, F., Resasco, D.E., Weisman, R.B. J. Am. Chem. Soc. 2003; 125: 11186-87.

79. Baker, R.T.K., Barber, M.A., Barber, P.S., Harris, P.S., Feates, F.S., Waite, R.J. J. Catal. 1972; 26: 51-62.

80. Baker, R.T.K., Harris, P.S., Henderson, F., Thomas, R.B. Carbon 1975; 13: 17-22.

81. Rodriguez, N.M. J. Mater. Res. 1993; 8: 3233-50.

82. Baker, H. Binary Alloy Phase Diagrams, vol. 3, ASM International, Materials Park, Ohio, 1992.

83. Reich, S., Thomsen, C., Maultzsch, J. Carbon Nanotubes: Basic Concepts and Physical Properties; Wiley-VCH: Weinheim, 2004; 31-65 pp.

84. Jiang, H., Nasibulin, A.G., Brown, D.P., Kauppinen, E.I. Carbon 2007; 45: 662-7.

85. Araujo, P.T., Maciel, I.O., Pesce, P.B.C., Pimenta, M.A., Doorn, S K., Qian, H., Hartschuh, A., Steiner, M., Grigorian, L., Hata, K., Jorio, A. Phys. Rev. B. 2008; 77: 241403-1-4.

86. Michel, T., Paillet, M., Nakabayashi, D., Picher, M., Jourdain, V., Meyer, J.C., Zahab, A.A., Sauvajol, J.-L. Phys. Rev. B 2009; 80: 245416-1-8.

87. Huang, S., Dai, L., Mau, A.W.H. Adv. Mat. 2002; 14: 1140-3.

88. Sener, S., Bilgen, S., Ozbayoglu, G. Miner. Eng. 2004; 17: 473-5.

89. Sevcik, V., Skvara, F. Ceram.-Silik. 2001; 45: 151-7.

90. Taylor, H.F.W. Cement chemistry (second ed.), Thomas Telford, London, 1997; 1 pp.

91. Nasibulina, L.I., Mudimela, P.R., Nasibulin, A.G., Koltsova, T.S., Tolochko, O.V., Kauppinen, E.I. Questions in Material Science (Voprosy Materialovedeniya) 2010; 61: 121-6.

92. Nasibulin, A.G., Brown, D.P., Queipo, P., Gonzalez, D., Jiang, H., Kauppinen, E.I. Chem. Phys. Lett. 2006; 417: 179-84.

93. Ivin, K.J., Mol, J.C. Olefin Metathesis and Metathesis Polymerization. 2nd ed. Academic Press: San Diego, 1997; 190-223 pp.

94. Magrez, A., Seo, J.W., Kuznetsov, V.L., Forro, L. Angew. Chem. Int. Ed. 2006; 46: 441-4.

95. Nasibulin, A.G., Brown D.P., Queipo, P., Gonzalez, D., Jiang, H., Kauppinen, E.I. Chem. Phys. Lett. 2006; 417: 179-84.

96. Dai, H., Rinzler, A., Nikolaev, P., Thess, A., Colbert, D., Smalley, R.E. Chem. Phys. Lett. 1996; 260: 471-6.

97. Pinheiro, P., Schouler, M.C., Gadelle, P., Mermouxb, M., Dooryhee, E. Carbon 2000; 38: 1469-79.

98. Queipo, P., Nasibulin, A.G., Jiang, H., Gonzalez, D., Tapper, U., Jiang, H., Tsuneta, T., Grigoras, K., Duenas, J.A., Kauppinen, E.I. Carbon 2006; 44: 1604-8.

99. Mondal, K., Lorethova, H., Hippo, E., Wiltowski, T., Lalvani, S.B. Fuel Process. Technol. 2004; 86: 33-7.

100.Boskovic, B.O., Stolojan, V., Khan, R.U.A., Haq, S., Silva, S.R.P. Nat. Mater. 2002; 1: 165-8.

101.Li, G.Y., Wang, P.M., Zhao, X. Cem. Concr. Compos. 2007; 29: 377-82.

102.Kowlad, T. Proc. Int. Symp. on Ultra High Performance Concrete, Germany, 2004; 195-203.

103.Makar, J.M., Beaudoin, J.J. Proc. of 1st Int. Symp. on Nanotechnology in Construction, Scotland, 2003; 246-58.

104.Xu, Y., Chung, D.D.L. Cem. Concr. Res. 1999; 29: 773-6.

105.Fu, X., Chung, D.D.L. Carbon 1998; 36: 459-62.

106.Fu, X., Lu, W., Chung, D.D.L. Carbon 1998; 36: 1337-45.

107.Li, G.Y., Wang, P.M., Zhao, X. Carbon 2005; 43: 1239-45.

108.Yu, X., Kwon, E. Smart Mater. Struct. 2009; 18: 055010-1-5.

ISBN 978-952-60-3454-6
ISBN 978-952-60-3455-3 (PDF)
ISSN 1795-2239
ISSN 1795-4584 (PDF)